frontiers | Frontiers in Molecular Biosciences

TYPE Original Research
PUBLISHED 10 November 2023
DOI 10.3389/fmolb.2023.1258799

OPEN ACCESS

EDITED BY
Martin Van Der Laan,
Saarland University, Germany

REVIEWED BY
Avia Rosenhouse-Dantsker,
University of Illinois Chicago,
United States
Tania C. B. Santos,
Weizmann Institute of Science, Israel

*CORRESPONDENCE
Gerald Gimpl,
gimpl@uni-mainz.de

†PRESENT ADDRESS
Lena Ahlswede,
Bayer Bitterfeld GmbH, Consumer Health, Bitterfeld, Germany

RECEIVED 14 July 2023
ACCEPTED 24 October 2023
PUBLISHED 10 November 2023

CITATION
Schiffmann A, Ahlswede L and Gimpl G (2023), Reversible translocation of acyl-CoA:cholesterol acyltransferase (ACAT) between the endoplasmic reticulum and vesicular structures.
Front. Mol. Biosci. 10:1258799.
doi: 10.3389/fmolb.2023.1258799

Reversible translocation of acyl-CoA:cholesterol acyltransferase (ACAT) between the endoplasmic reticulum and vesicular structures

Andrea Schiffmann, Lena Ahlswede† and Gerald Gimpl*

Department of Chemistry and Biochemistry, Biocenter II, Johannes Gutenberg University Mainz, Mainz, Germany

The enzyme acyl-CoA:cholesterol acyltransferase (ACAT) is normally localized in the endoplasmic reticulum (ER) where it can esterify cholesterol for storage in lipid droplets and/or the formation of lipoproteins. Here, we report that ACAT can translocate from the ER into vesicular structures in response to different ACAT inhibitors. The translocation was fast (within minutes), reversible and occurred in different cell types. Interestingly, oleic acid was able to fasten the re-translocation from vesicles back into the reticular ER network. The process of ACAT translocation could also be induced by cyclodextrins, cholesterol, lanosterol (but not 4-cholestene-3 one), 25-hydroxycholesterol, and by certain stress stimuli such as hyperosmolarity (sucrose treatment), temperature change, or high-density cultivation. *In vitro* esterification showed that ACAT remains fully active after it has been translocated to vesicles in response to hyperosmotic sucrose treatment of the cells. The translocation process was not accompanied by changes in the electrophoretic mobility of ACAT, even after chemical crosslinking. Interestingly, the protein synthesis inhibitor cycloheximide showed a stimulating effect on ACAT activity and prevented the translocation of ACAT from the ER into vesicles.

KEYWORDS

acyl-CoA:cholesterol acyltransferase (ACAT), bovine serum albumin (BSA), cycloheximide (CHX), disuccinimidyl suberate (DSS), cholesterol ester (CE), dansyl-cholestanol (DChol), free cholesterol (FC), ACAT inhibitor (iACAT)

Introduction

In cells, the majority (60%–90%) of total cholesterol is localized in the plasma membrane (Lange et al., 1989; Ikonen, 2008; van Meer et al., 2008) where it is organized in different pools (Radhakrishnan and McConnell, 2000; Ohvo-Rekila et al., 2002; Lange et al., 2004; Lange et al., 2013; Das et al., 2014). Only a small fraction of 'active' cholesterol that is not

Abbreviations: ACAT, acyl-CoA:cholesterol acyltransferase; BSA, bovine serum albumin; CHX, cycloheximide; DSS, disuccinimidyl suberate; CE, cholesterol ester; DChol, Dansyl-cholestanol; FC, free cholesterol; iACAT, ACAT inhibitor; INSIG, insulin-induced gene protein; MAM, mitochondria associated membrane; MβCD, methyl-β-cyclodextrin; MLX, Max-like protein X; OA, oleic acid; SREBP, sterol response element binding protein; SOAT, sterol O-acyltransferase; SCAP, SREBP cleavage-activating protein; TAG, triacylglycerol.

complexed with other lipids (in particular sphingomyelin) can move to the endoplasmic reticulum (ER) by a non-vesicular pathway using transfer proteins of the Aster (=GramD) family (Sandhu et al., 2018; Naito et al., 2019). As a co-ligand of the Aster proteins, phosphatidylserine also plays a central role in this protein-mediated transfer of cholesterol from the plasma membrane to the ER (Trinh et al., 2020; Ercan et al., 2021; Trinh et al., 2022). The ER contains only small amounts of total cholesterol and functions as the cholesterol sensing compartment where key components of the cholesterol homeostatic machinery (SREBP-SCAP-INSIG) are localized (Brown et al., 2018). Any influx of cholesterol into the ER exceeding a threshold value of ~5 mol% activates this feedback system.

To prevent the accumulation of free cholesterol, which is toxic to cells, cholesterol is esterified by acyl-CoA:cholesterol acyltransferase (ACAT). ACAT enzymes are also known as sterol O-acyltransferases (SOATs) and exist in two isoforms, ACAT1 and ACAT2. ACAT1/SOAT1 is ubiquitously expressed in nearly all tissues to maintain cholesterol homeostasis, whereas ACAT2 is mainly found in the liver and intestine (Rogers et al., 2015). They both catalyse the formation of cholesterol esters (CE) from cholesterol and long-chain or medium-chain fatty acids. These esters are either stored in lipid droplets or are secreted as lipoproteins (Chang et al., 2001a; Chang et al., 2001b; Lin et al., 2003). ACAT enzymes are membrane proteins residing in the endoplasmic reticulum (ER). However, it is important to mention that a localization of ACAT1 distinct from the ER has also been demonstrated under some conditions and/or in some cell types (Khelef et al., 2000; Sakashita et al., 2010; Kamikawa et al., 2014). Despite its key role in the cellular sterol homeostasis, the sterol regulation of ACAT1 does not occur at the transcriptional level, as the gene promoter lacks sterol response elements (Chang et al., 1998; Chang et al., 2001a). ACATs are allosteric enzymes that form tetramers and can be activated by a variety of sterols. According to one model, ACAT1 contains two different binding sites for steroidal molecules, a substrate and an activator site (Rogers et al., 2012; Rogers et al., 2015). Recent structural data confirmed the dimerization/tetramerization of ACAT1 (Guan et al., 2020; Qian et al., 2020). Interestingly, ER-resident ACAT1 was shown to esterify also cholesterol metabolites which are produced in the mitochondria such as pregnenolone and some oxysterols (Rogers et al., 2015). This raises the question of where and how the enzyme interacts with these substrates. Notably, ACAT1 was reported to be enriched in a sub-compartment of the endoplasmic reticulum (ER), the so-called mitochondria-associated membranes (MAMs) (Area-Gomez et al., 2012). These structures are physically and biochemically connected to mitochondria and could possibly enable direct molecular contacts of enzyme and substrate. But this hypothesis remains to be tested.

In this study, we explored the intracellular distribution profile of ACAT1/SOAT1 under various conditions. Thereby, we observed a significant translocation of the enzyme out of the extensive ER network into vesicular structures in response to certain stimuli. This translocation process was rapid and reversible and could be a way to regulate cholesterol esterification in cells, by altering the accessibility of the enzyme to its substrate. Finally, the results of this study also shed new light on the mechanisms of ACAT inhibitors and may help to explain previous observations regarding the localization profile and the activity of ACAT1/SOAT1.

Results

The fluorescent cholesterol analogue DChol and the fatty acid probe Bodipy-C12-568 are reporters of ACAT activity

We have introduced DChol (Figure 1A) as a valuable reporter of cholesterol trafficking in cells (Wiegand et al., 2003). DChol and cholesterol can easily be incorporated into methyl-β-cyclodextrin (MβCD) cages to form efficient sterol-MβCD donor complexes. This allows rapid sterol delivery to the cells. When CHO cells pulse-labeled with DChol-MβCD were incubated for 24 h in culture medium and then processed for lipid extraction, substantial amounts of DChol were found to be esterified as shown by thin layer chromatography (TLC) and subsequent fluorescence detection (Figure 1B). The DChol-ester spot was absent when the cells were treated in the presence of SAN 58-035, an ACAT inhibitor (iACAT) (Veldhuis et al., 1985) (Figure 1B). This proves the ACAT specificity of the DChol-ester formation. Esterification of cholesterol was determined in the same manner in additional cells: HEK, HeLa, HepG2, Saos2 and (as a negative control) ACAT-deficient AC29 cells (Figure 1C). Following TLC separation of the lipid extracts, the ratios of esterified to free DChol were calculated, showing the highest esterification activity for HeLa and the lowest for Saos2 cells (Figure 1C).

DChol moves from the plasma membrane to the endoplasmic reticulum (ER) and is then finally transported to lipid droplets where it is stored in form of DChol-ester. This process requires ACAT activity (Wiegand et al., 2003). We therefore expected that overexpression of ACAT should accelerate this storage process. To test this hypothesis, we conducted an experiment in which HEK293 cells stably expressing EGFP-tagged ACAT1 (termed HEK-ACAT) were mixed with non-transfected HEK293 cells. The cells were pulse-labeled with DChol-MβCD and co-cultivated in medium. After 5 h of incubation, DChol was mainly found in ER structures in non-transfected cells whereas in cells overexpressing ACAT, lipid droplets containing DChol were clearly present (Figure 1D, compare left and middle image). To quantitate this process, DChol-labeled lipid droplets in transfected *versus* non-transfected cells were counted. In the right panel of Figure 1D, such a quantification is shown for three single cells (compare non-transfected cell #1 with ACAT overexpressing cells #2 and #3). Thus, the development of DChol containing lipid droplets was significantly accelerated in cells that overexpress ACAT. Under the same experimental conditions, the formation of DChol-labled lipid droplets occurred ~4 h earlier in HEK cells overexpressing ACAT compared with non-transfected HEK cells (Figure 1E). After an incubation time of 8 h, roughly equal amounts of lipid droplets were visible in non-transfected *versus* ACAT overexpressing HEK cells. In the presence of an ACAT inhibitor, the appearance of lipid droplets was completely suppressed during the time course of the experiment (Figure 1E). Similarly, the appearance of ACAT specific DChol-labeled lipid droplets also occurred in other cell types. Specifically, after 8 h, an ACAT-dependent formation of DChol containing lipid droplets was observed in CHO and in COS-7 cells (Figure 1F).

The esterification of cholesterol also requires a continuous supply of fatty acids. The incorporation of a fluorescent fatty acid

10.3389/fmolb.2023.1258799

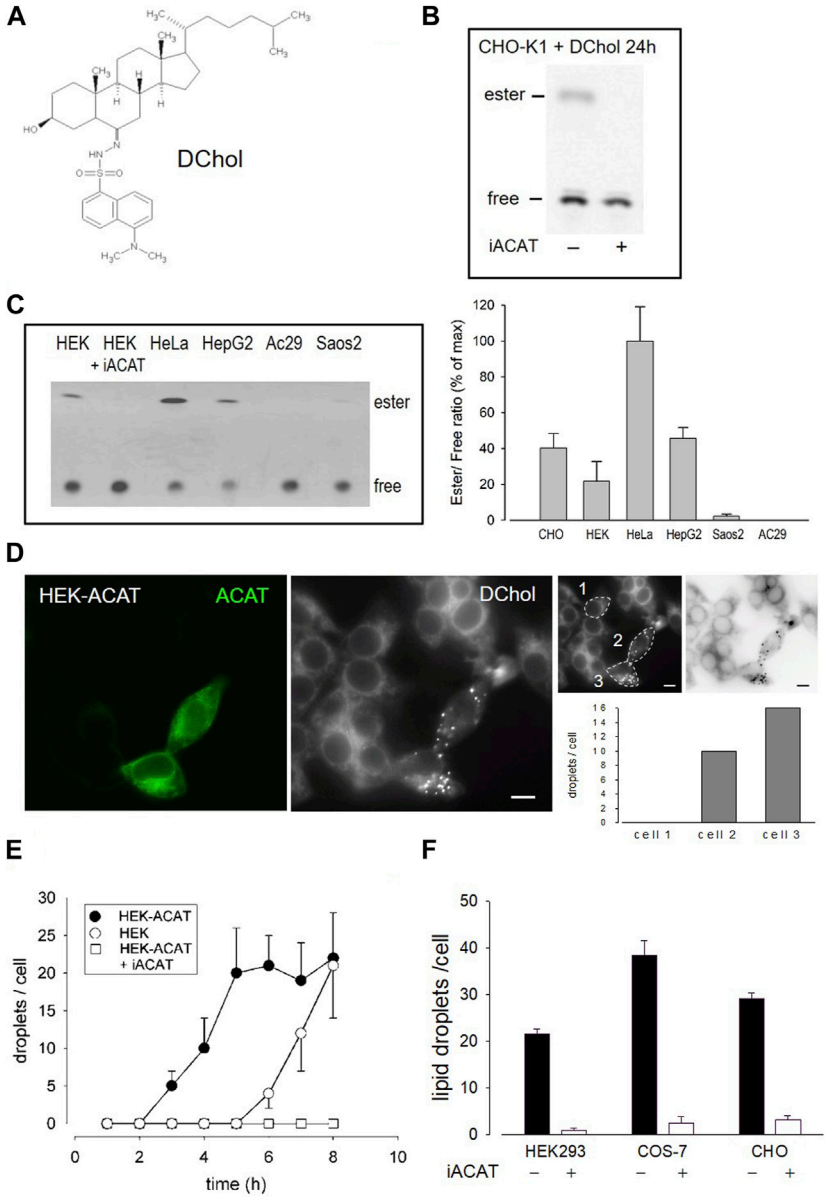

FIGURE 1
DChol is esterified by ACAT. **(A)** Structure of DChol. **(B)** CHO-K1 cells were pulse-labeled for 1 h with DChol-MβCD (7 μM) in culture medium in the absence or presence of the ACAT inhibitor SAN 58-035 (iACAT) (0.4 μg/mL). The medium was washed off and chasing was performed for the indicated time. The cells were harvested and their lipids were extracted and separated by silica gel TLC using heptane/diethyl ether/methanol/acetic acid (80:30:3: 1.5, by vol) as mobile phase. The fluorescence of free or esterified DChol was detected under UV light. **(C)** The DChol esterification of other cells (HEK, HeLa, HepG2, Saos2, AC29) were performed as described above. The ratio of DChol ester to free DChol was quantified by fluorimetry (right panel). Data are means ± SD of three experiments. Values for HeLa (0.41 ± 0.08, set to 100%) were significantly higher than those of HepG2 ($p = 0.0035$) and all other cells ($p < 0.001$). **(D)** Increase of ACAT activity accelerates the formation of DChol/ester containing lipid droplets. HEK293 cells stably expressing GFP-tagged ACAT1 (HEK-ACAT) were mixed with untransfected HEK293 cells, were co-cultivated for 24 h, and were incubated for 10 min with culture medium containing DChol-MβCD (10 μM). After removal of the medium, the cells were cultivated for 5 h and then observed by fluorescence microscopy. Left image, ACAT; middle image, DChol; right images, quantification of the number of lipid droplets in cell #1 (control), and cells #2 and #3 that overexpress ACAT (bar, 10 μm); data from a representative experiment ($n = 6$). **(E)** HEK cells (○), HEK-ACAT cells in the absence (□) or presence (●) of iACAT were labeled for 10 min with DChol-MβCD (10 μM). Thereafter, the cells were incubated for the indicated times and the number of lipid droplets were counted ($n > 50$ cells for one experiment performed in triplicate; means ± SD). **(F)** HEK, COS-7, and CHO cells were labeled for 10 min with DChol-MβCD (10 μM) in the presence or absence of iACAT. After a further incubation of 8 h in culture medium, the DChol containing lipid droplets were counted ($n > 50$ cells in one representative experiment; means ± SD).

could therefore also report on the formation of DChol esters. For this purpose, we performed labeling experiments with the fatty acid probe Bodipy-C12-568 in AC29 cells which are mutant CHO cells deficient in endogenous ACAT activity. AC29 cells stably transfected with AcGFP-ACAT1 (termed AC29-ACAT cells) were pulse-labeled for 10 min with Bodipy-C12-568. After washing and chasing the cells for 3 h with culture medium, the cells were analyzed by fluorescence microscopy. As shown in

10.3389/fmolb.2023.1258799

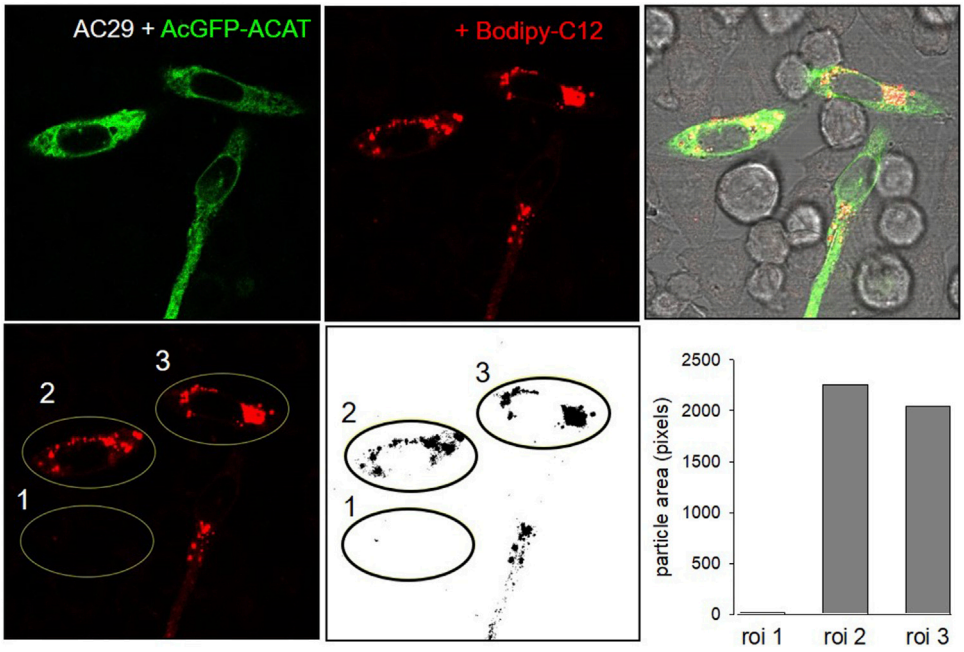

FIGURE 2
ACAT esterification incorporates fatty acids into lipid droplets. CHO cells that are deficient in ACAT activity (AC29) were transfected with AcGFP-ACAT and were labeled for 10 min with the fatty acid probe Bodipy-C12-568. After a washing step, the cells were incubated in culture medium for 3 h and analyzed by fluorescence microscopy. Upper images: left, AcGFP-ACAT; middle, Bodipy-C12-568; right, overlay including bright field. Lower images: quantification of the Bodipy-C12-568 image using 3 regions of interests (roi); the image was thresholded, binarized and processed for particle counting (ImageJ, NIH). Data from a representative experiment (n = 4).

Figure 2, only the three ACAT expressing cells (left upper image) have incorporated substantial amounts of Bodipy-C12-568 (middle upper image and right overlay image). The quantification of these signals in 3 regions of interest (roi) (Figure 2, lower images: #1, non-transfected cell; #2 and #3, transfected cells) revealed large differences (~150 fold) in the fluorescence of the fatty acid probe between ACAT expressing and non-transfected cells. Thus, the incorporation of Bodipy-C12-568 was found to be an excellent and sensitive reporter assay to calculate the ACAT activity in living cells.

ACAT translocates from the ER to vesicular structures in response to ACAT inhibitors

Under normal physiological conditions, ACAT1 is localized in the widespread ER network. To visualize the ER, the large and flat-shaped fibroblast-like COS-7 cells were stably transfected with EGFP-tagged ACAT1 and were labeled with DChol-MβCD. After several hours of incubation, abundant DChol-containing lipid droplets developed, mostly associated with ER tubules in which ACAT was present (Supplementary Figure S1). The majority of the DChol-labeled droplets remain closely connected with the ER as shown in Supplementary Figure S1 for one single lipid droplet marked with arrowhead. Formation of lipid droplets most likely occurs through a budding process at the ER and often continue to adhere to the ER membrane after biogenesis (Murphy and Vance, 1999; Brown, 2001; Targett-Adams et al., 2003; Walther et al., 2017; Olzmann and Carvalho, 2019).

To our great surprise, the distribution profile of ACAT changed dramatically after an ACAT inhibitor (iACAT) was added to the cells (Figure 3). In our first experiments, we have added the ACAT inhibitor SAN 58035 at 0.4 μg/mL for 1 h to HEK-ACAT cells. In nearly all cells, ACAT translocated from the ER (Figure 3A) to predominantly vesicular structures (Figure 3B). When iACAT was applied for several hours, ACAT was occasionally observed in cluster-like structures in a couple of cells (Figure 3C). To exclude the possibility that the ACAT inhibitor induces changes in the ER network in any way, the effect of iACAT was tested on HEK293 cells cotransfected with EGFP-ACAT1 and the ER marker DsRed-ER. While ACAT was again found in vesicular structures, no significant alterations in the ER network were detected (Figure 3D). In addition, an antibody against the ER resident protein calnexin did not indicate structural changes in the ER in response to ACAT inhibition (Figure 3E).

Next, we assessed whether the translocation of ACAT also occurs in other cells. Both, the CHO-derived AC29 as well as HeLa cells, each transfected with EGFP-tagged ACAT showed a prominent ACAT translocation following the application of ACAT inhibitor SAN 58035 (0.4 μg/mL) for 1 h (data not shown). To rule out the possibility, that adding the EGFP-tag could have led to undesired dimerization/oligomerization of ACAT, we substituted the EGFP-tag by monomeric AcGFP and expressed this construct in AC29 cells. But, AcGFP-tagged ACAT behaved the same way. Following ACAT inhibition, it moved from the ER to vesicles (Supplementary Figure S2).

Next, we tested whether the observed translocation behavior of ACAT is a specific response to SAN 58-035 or can also be induced by

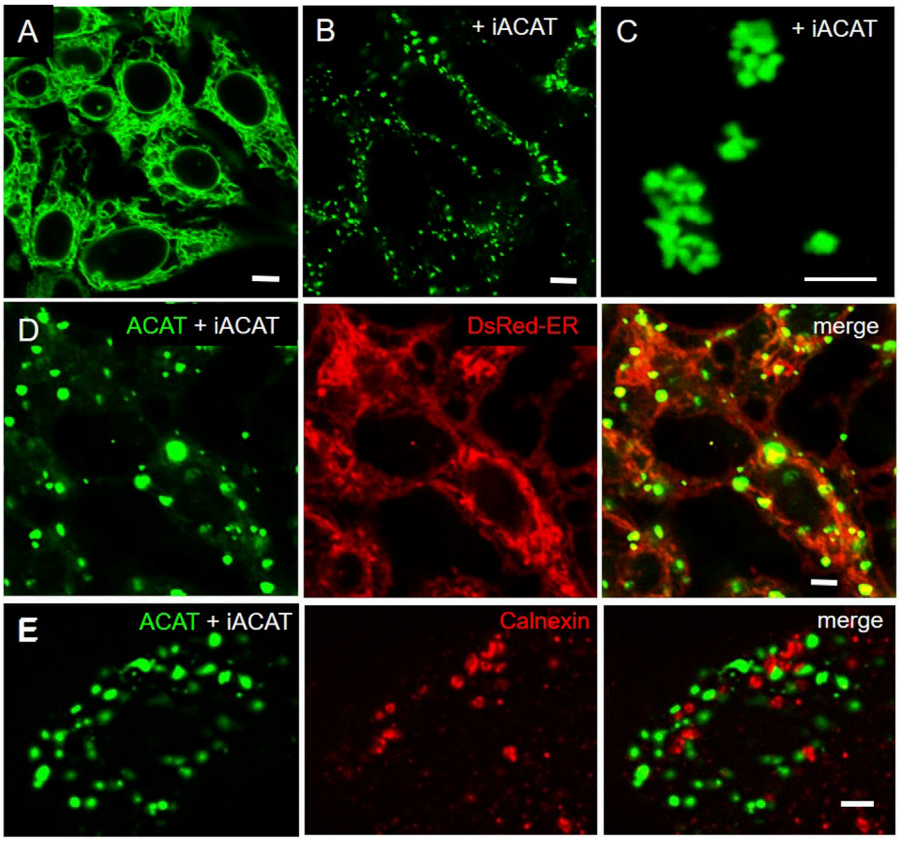

FIGURE 3
Inhibition of ACAT induces significant changes in its intracellular distribution. HEK-ACAT cells **(A–C,E)** or HEK cells stably cotransfected with ACATGFP and DsRed-ER **(D)** were treated **(B–E)** or not treated **(A)** for 1 h **(B,D,E)** or 4 h **(C)** with the ACAT inhibitor SAN 58035 (0.4 μg/mL) in a microscope chamber at 30°C. Following application of the inhibitor, a predominant vesicular pattern of ACAT **(B,D,E)** is observed in most cells. After prolonging the incubation time to several hours, additional cluster-like structures are occasionally found in some cells **(C)**. **(E)** Formaldehyde-fixed and permeabilized cells were stained with anti-calnexin/anti-mouse-IgG-Cy3. The ER structure (in D and E) did not change significantly after application of iACAT. Images from a representative experiment (n = 4) (bars, 5 μm).

TABLE 1 Effects of ACAT inhibitors on ACAT translocation event. AC29-ACAT cells were treated with the indicated compounds and were then inspected for ACAT1 translocation. The extent of translocation is indicated by symbols: (+++), massive formation of vesicles in virtually every cell; (++), vesicle formation in >80% of cells; (+) weak translocation or translocation in only a fraction of cells; (–) no effect.

Compound	Treatment (concentration, time)	Translocation	References
SAN 58035	0.8 μM, 1 h	+++	Veldhuis et al. (1985)
Eflucimibe	0.4 μM, 30 min	+++	Junquero et al. (2001a)
Tamoxifen	10 μM, 1 h	+++	de Medina et al. (2004)
Avasimibe	10 μM, 1 h	++	Lee et al. (1996)
Auraptene	10 μM, 1 h	+	de Medina et al. (2010)
Piperine	20 μM, 1 h	+	Matsuda et al. (2008)

other ACAT inhibitors. The following additional compounds were used: eflucimibe (=F12511) (Junquero et al., 2001b), avasimibe (Lee et al., 1996), auraptene (de Medina et al., 2010), piperine (Matsuda et al., 2008), and tamoxifen (de Medina et al., 2004). As shown in Table 1, all these compounds caused ACAT translocation, albeit to varying degrees. While SAN 58035, eflucimibe, tamoxifen, and avasimibe were most effective, auraptene and piperine induced ACAT translocation in only a fraction of cells. Among all compounds tested so far, eflucimibe was effective at the lowest concentration and caused a maximum effect in the shortest time. For this reason, we used eflucimibe in most further experiments.

Overall, we did not detect a strong colocalization of the ACAT containing vesicles (or cluster structures) with known organelle markers (Supplementary Figures S3, S4). To quantify the

10.3389/fmolb.2023.1258799

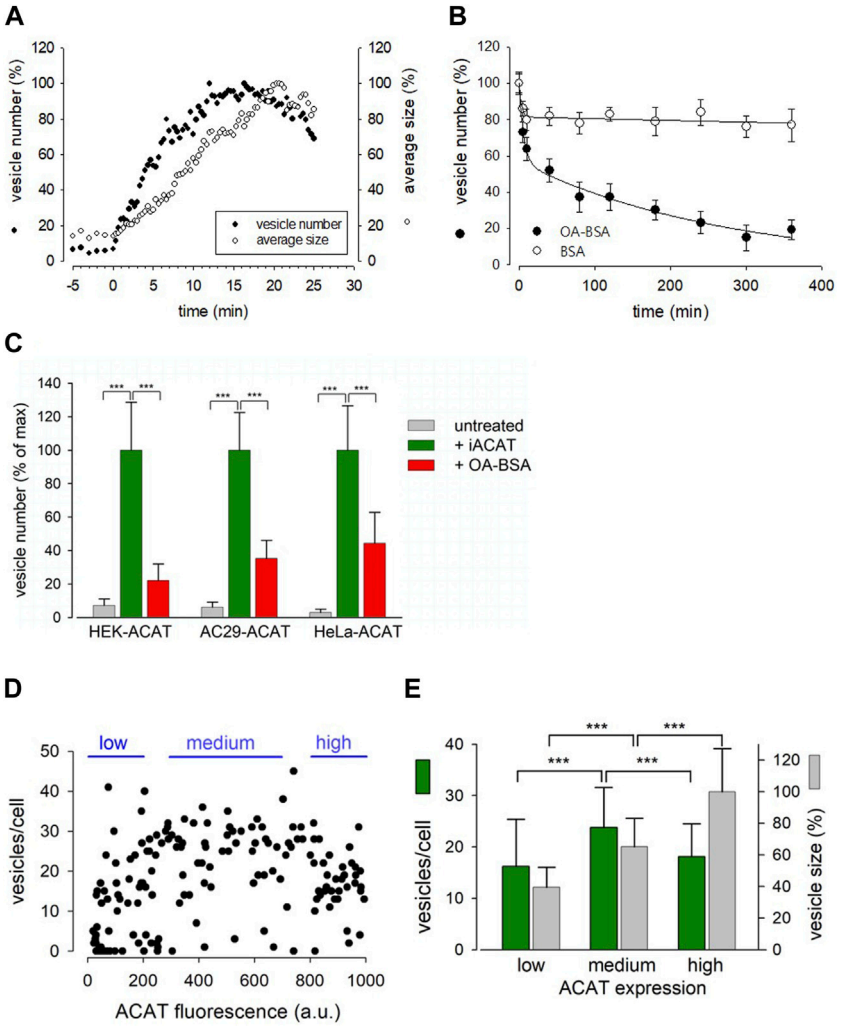

FIGURE 4
Characterization of the Eflucimibe-induced ACAT translocation. HEK-ACAT **(A–E)**, AC29-ACAT **(C)** and HeLa-ACAT cells **(C)** were cultivated in a temperature controlled microchamber on the microscope stage. The translocation of ACAT was initiated with ACAT inhibitor eflucimibe (0.5 μM). **(A)** About 5 min after application of eflucimibe, the number (●) and size (o) of ACAT containing vesicles were determined. Images were captured each 20 s starting at time 0. The vesiculation process was quantified by using the particle counting module of ImageJ (NIH). Data are from a representative experiment (15–20 cells per field of view, 100% level corresponds to maximum number of vesicles (~400) (n = 3). **(B)** Eflucimibe was washed-off after 30 min, and the reversibility of the vesiculation was initiated by addition of BSA (10%) (o) or BSA-bound oleic acid (400 μM OA in 10% BSA) (●). The number of vesicles decreased as determined by imaging and particle counting at different times. The data are means ± SD and were fitted by exponential functions: double exponential (with 4 parameters) for BSA: a = 18.63, b = 0.321, c = 81.457, d = 0.0001184; for OA-BSA: a = 42.83, b = 0.171, c = 56.94, d = 0.0037. **(C)** The number of vesicles before treatment (untreated, grey bars) and after 30 min of treatment with eflucimibe (+iACAT, green bars) was counted in the indicated cells. Then, eflucimibe was washed-off and the reversibility of the vesiculation was measured after 5 h of treatment with oleic acid-BSA (OA-BSA, red bars). Data are means ± SD (n = 3) (80–100 cells, with 15–20 cells per field of view). The corresponding 100% levels of vesicles/cell were: 23.7 ± 6.8 (HEK-ACAT), 26.2 ± 5.9 (AC29-ACAT), and 32.5 ± 8.7 (HeLa-ACAT). Cells that did not show significant eflucimibe-induced ACAT vesiculation ("non-responder cells" with <3 vesicles/cell) were ~8% for HEK-ACAT, ~10% for AC29-ACAT, ~14% for HeLa-ACAT. **(D)** A mixture of HEK-ACAT cells stably expressing ACAT at different levels was treated with eflucimibe for 30 min. Number and size of vesicles in individual cells were quantified by particle counting and were correlated with the EGFP fluorescence as an indicator of the expression level of ACAT. Each point represents data from a single cell (161 cells). Number and size of vesicles in cells expressing low (0–200 a.u., 44 cells, 14 non-responder cells), medium (300–700 a.u., 47 cells, 3 non-responder cells), and high (800–1000 a.u., 38 cells, 2 non-responder cells) ACAT amounts are indicated in the bar graph **(E)**. *** in **(C,E)** indicates $p < 0.001$ (t-test).

association between ACAT vesicles and marker staining, Pearson correlation coefficients were calculated not only for the overall distribution of the signals averaged over many cells, but also in selected smaller "regions of interest" where ACAT vesicles and the corresponding markers appear to be colocalized after visual inspection. Regions with smaller vs. larger ACAT vesicles were also considered. The highest, although still very moderate colocalization was obtained for peroxisomes (with a Pearson's coefficient of r = 0.42 ± 0.07) employing DsRed-Peroxi as the organelle marker (Supplementary Figure S4B). Pearson coefficients close to zero or below zero were observed for the markers for Golgi (anti-Golgin in Supplementary Figure S3B and WGA-TR in Supplementary Figure S3C) and ER exit sites (anti-Sec31 in Supplementary Figure S4C), i.e., ACAT vesicles are neither

10.3389/fmolb.2023.1258799

Golgi vesicles nor ER exit sites as no colocalization with their compartment markers was observed. Both Lysotracker (r = 0.15 ± 0.06) (Supplementary Figure S3A) and mitotracker (r = 0.11 ± 0.05) (Supplementary Figure S4A) staining showed a slight positive correlation with ACAT vesicles. In selected "regions of interest" where ACAT vesicles are close to mitochondria or where the ACAT vesicles are larger in size, higher Pearson coefficients could be measured for both lysotracker (r = 0.24 ± 0.06) and mitotracker (r = 0.21 ± 0.07). Taken together, ACAT vesicles show moderate colocalization with peroxisomes and a weak colocalization with mitochondria and lysosomes. The latter was significantly more pronounced in selected regions of the cells where larger ACAT vesicles were frequently located.

ACAT translocation is fast and reversible, but can be prevented by cycloheximide

We now studied the kinetics of ACAT translocation in HEK-ACAT cells in response to eflucimibe. Approximately 5 min after ACAT inhibitor administration, both the number and size of ACAT-containing vesicles began to increase (Figure 4A). About 15 min later, the number of vesicles reached its maximum (Figure 4A, filled circles). However, the size of the vesicles/clusters further increased for a few more minutes (Figure 4A, open circles). When eflucimibe was washed off, the number of vesicles began to decrease, albeit at a very low rate. Even after 7 h of incubation without eflucimibe, nearly 80% of the ACAT vesicles were still present (Figure 4B, open circles). To minimize phototoxicity and photobleaching, the cells were excited only at the indicated time points using low laser intensity (~10% of maximum laser power). However, we also observed similar results in terms of number and size of ACAT vesicles when we greatly increased the exposure intervals, e.g., to only one exposure every 3 min, i.e., with about 10-fold less excitation time (not shown). Thus, we exclude a significant influence of the phototoxicity on the degree of ACAT vesiculation.

This prompted us to test if certain substances are able to accelerate the reversibility of the translocation process. In the process, we tried oleic acid as a candidate, as its activated form, oleoyl-CoA, is a preferred cellular substrate of ACAT (Chang et al., 2010). Surprisingly, we found that the administration of oleic acid complexed with BSA dramatically increased the re-translocation process of ACAT from vesicular structures into the ER compartment. In less than 5 h, roughly 80% of the vesicles had disappeared (Figure 4B, filled circles). Both, eflucimibe-induced vesiculation of ACAT and oleic-acid accelerated reversibility of this process were also observed in AC29-ACAT and HeLa-ACAT cells (Figure 4C, green and red bars). In cells that did not receive eflucimibe prior to administration of oleic acid-BSA (for 5 h), ACAT resided unaltered within the reticular ER (Figure 4C, grey bars). The concentration of 400 µM oleic acid in complex with BSA was used because it is commonly applied in experiments where the formation of lipid droplets is to be induced. We have also tested the reversibility of vesicle formation at lower concentrations of oleic acid-BSA complexes. Equally-fast kinetics of reversion as with 400 µM was obtained with 100 µM oleic acid. At 10 µM oleic acid, the kinetics of the reversion was significantly slowed, while no significant

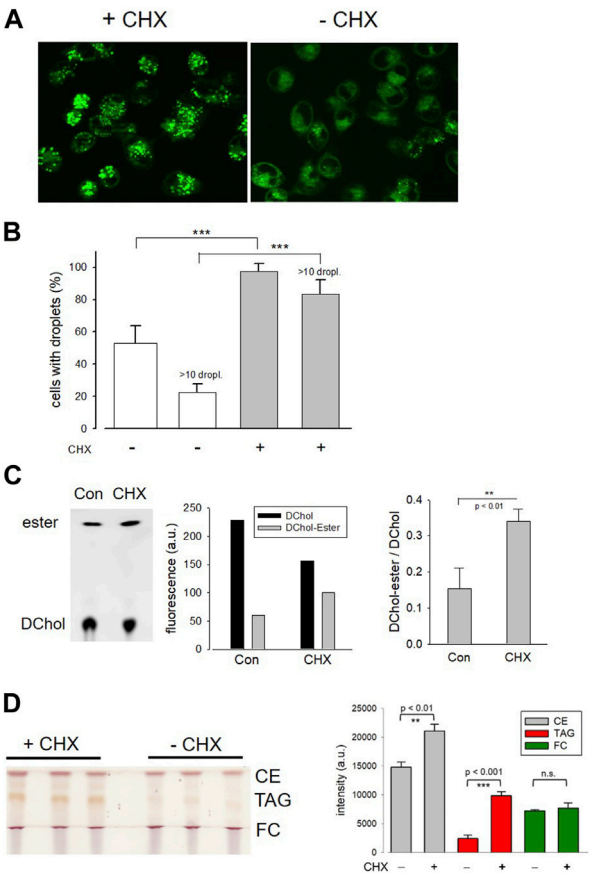

FIGURE 5
Effect of cycloheximide on lipid droplet formation and cholesterol esterification. **(A)** HeLa cells grown on glass-bottom dishes were incubated for 12 h in the presence (+CHX) or absence (-CHX) of cycloheximide (20 µM) in DMEM without FCS. Thereafter, Bodipy 493/503 (4 µM) was added for 30 min. After a washing step, the cells were imaged and droplets were counted **(B)** as described (-CHX, 89 cells; +CHX, 100 cells; $n = 3$; means ± SD; ***, $p < 0.001$). **(C)** HeLa cells cultivated in Petri dishes were incubated for 14 h with DChol-MβCD (0.3 mM) in the absence (Con) of presence of cycloheximide (CHX) (20 µM) in DMEM (with FCS). The cells were harvested, and the corresponding lipid extracts were analyzed by TLC. Free and esterified DChol was quantitated by fluorimetry using the imaging device UVP ChemStudio (Analytic-Jena). The quantitation of a representative TLC (left panel) is shown in the middle panel of the graph. The right panel shows the ratio of DChol-Ester to DChol (means ± SD) obtained in three independent experiments. **(D)** HeLa cells were cultivated in Petri dishes in the absence (Con) or presence of cycloheximide (CHX) (20 µM) in DMEM (with FCS). The cells were harvested, and the corresponding lipid extracts were separated by TLC. The air dried plate was sprayed with sulfuric acid:methanol (1:1 vol%) and heated at 120°C for 5 min. Free cholesterol (FC), cholesteryl ester (CE), and triacylglycerols (TAG) were quantitated by ImageJ. The data are mean values ± SD (right panel) from the corresponding lipid bands shown in the left panel ($n = 2$).

acceleration of this reversion process was observed at 1 µM oleic acid compared to the BSA control (not shown). Thus, oleic acid concentrations of at least 10 µM were required to induce the reversibility of the vesiculation process. However, it is important to mention that the study of this process is largely influenced by the slow washout of the ACAT inhibitor.

To test whether and how overexpression of ACAT affects the translocation process, a mixture of HEK-ACAT cells expressing the

protein at different levels was stimulated to form vesicles by eflucimibe (30 min). In individual cells, the number and size of ACAT vesicles were quantified and were correlated with the EGFP fluorescence as an indicator of ACAT expression level. As shown in Figures 4D, E, cells with a wide range of ACAT expression levels were capable of ACAT translocation, with some specific differences. For example, the mean vesicle size was found to increase with the expression of ACAT, whereas the number of vesicles was highest at intermediate expression levels (Figure 4E). It was further observed that the expression level of ACAT increased the probability of triggering ACAT translocation. Approximately 30% of cells expressing low levels of ACAT showed no vesicle formation, while this proportion was reduced to only 5%–6% in cells with higher expression levels.

Conclusively, the translocation process of ACAT was relatively fast, occurring within minutes, and was reversible. In addition, it could be triggered twice in succession on the same cells.

In further experiments, we surprisingly found that the pretreatment of cells with the protein synthesis inhibitor cycloheximide prevented the translocation of ACAT in vesicles. Interestingly, it has been reported that cycloheximide can induce the formation of cholesterol ester-rich lipid droplets (Suzuki et al., 2012). This suggests that ACAT could be somehow activated by cycloheximide. In fact, when HeLa cells were incubated with cycloheximide (for 12 h at 20 μM), the number of lipid droplets significantly increased as shown by the fluorescence marker Bodipy 493/503 (Figure 5A). After treatment with cycloheximide (CHX), lipid droplets were observed in approximately twice as many cells, with droplet-rich cells (>10 droplets) being as much as 4 times more abundant than in untreated cultures (Figure 5B). Subsequently, it was tested whether the higher number of lipid droplets in CHX-treated cells was also associated with an increased rate of cholesterol esterification. The lipid extracts of HeLa cells that were incubated with the ACAT substrate DChol in the presence or absence of cycloheximide were analyzed by TLC. Free and esterified DChol was quantitated by fluorimetry. The quantitation of a representative TLC (Figure 5C, left panel) is shown in the middle panel of the graph. The right panel in Figure 5C shows the ratio of DChol-Ester to DChol obtained in three experiments with HeLa cells in the presence and absence of cycloheximide, respectively. Significantly higher amounts of DChol esters were formed in the cycloheximide-treated cells than in untreated cells. Finally, the lipid extracts from HeLa cells treated or untreated with cycloheximide were separated by TLC, and the resolved lipid species were visualized by heating after spraying with sulfuric acid:methanol (Figure 5D). Each of the bands corresponding to free cholesterol (FC), cholesterol esters (CE), and triacylglycerols (TAG) were quantitated and are displayed as mean values ± SD in Figure 5D (right panel). These data show that, in addition to cholesterol esters, particularly the formation of triacylglycerols was increased in cycloheximide-treated cells, approximately fourfold compared with control cells.

ACAT translocation can also be induced by other substances and stimuli

Next, it was explored whether other substances or treatments could also induce intracellular translocation events of ACAT. The results are shown in summarized form in Table 2. First, the cholesterol content of HEK-ACAT cells was decreased or increased by incubation with the cholesterol acceptor methyl-β-cyclodextrin (MβCD) or the water-soluble inclusion complex cholesterol-MβCD, respectively. In both cases, a massive translocation of ACAT from ER into vesicles occurred. Since MβCD itself was able to induce ACAT translocation, the specificity of the effect of cholesterol-MβCD was not possible to judge. Therefore, we additionally used cholesterol dissolved in ethanol, which caused a significant ACAT translocation at concentrations >30 μM. A similarly strong effect was achieved when the sterol analogue lanosterol was used. In contrast, the steroid cholesten-3-one was ineffective under the same experimental conditions. Among other substances that are known to affect the cholesterol homeostasis (25-hydroxycholesterol, lovastatin, U18666A) only 25-hydroxycholesterol was able to induce a slight translocation of ACAT. Osmotic stress induced by administration of sucrose also lead to a substantial translocation of ACAT into vesicles. Other substances that are known to interfere with microtubule polymerization (nodocazole), ER to Golgi transport (brefeldin A), or cellular signaling (forskolin, H89, phorbol ester, lysophosphatidic acid, Y27632, wortmannin, U73122) did not alter the intracellular localization of ACAT (Table 2).

We always used 30°C for live cell microscopy. However, it is important to note that we did not observe any qualitative changes in vesicle formation between 30°C and 37°C. Interestingly, we also noticed that ACAT translocation was facilitated or promoted spontaneously when the cells were exposed to a lower temperature (at ~23°C and below, e.g., by transfer from 37°C to room temperature), especially when cells were cultivated at maximum density. Despite many efforts, we have not been able to define the exact conditions that reproducibly lead to spontaneous ACAT vesicle formation. However, the induced translocation of ACAT, e.g., by administration of an ACAT inhibitor, was always possible at 25°C and higher temperatures.

The translocation process is not accompanied by changes in electrophoretic mobility of ACAT

The question arises whether the translocation of ACAT is accompanied by molecular alterations of the protein such as oligomerization, aggregation or proteolysis. First, the migration behavior of endogenous ACAT in SDS-PAGE (Figure 6A, left lanes) was analyzed. HEK293 cells treated or not treated with eflucimibe (0.5 μM, 1 h) were homogenized, and the proteins were separated by SDS-PAGE, followed by immunoblotting with anti-ACAT/SOAT antibody. The endogenous ~50 kDa monomeric anti-ACAT species is running at a slightly lower than predicted molecular weight (~64 kDa). This differential migration pattern of ACAT is known from earlier studies and was assumed to be caused by the high IEP (~8.7) of the protein (Cheng et al., 1995). In the presence of eflucimibe, the electrophoretic mobility of endogenous ACAT did not change (Figure 6A, left lanes). Even when protein analysis was performed using native/non-denaturing conditions with HEK-ACAT cells, eflucimibe induced no alterations in the gel mobility of ACAT (Figure 6A, right lanes).

We also studied the electrophoretic mobility of ACAT using AC29-ACAT cells and incubated in the absence (control) or

TABLE 2 Effects of substances or treatments on ACAT translocation. HEK-ACAT cells were treated with the indicated compounds and were then inspected for ACAT1 translocation. The symbols indicate: (++), vesicle formation in >80% of cells; (+) weak translocation or translocation in only a fraction of cells; (–) no effect.

Compound	Effect	Treatment	Translocation
Cholesterol-MβCD	Cholesterol increase	0.3 mM, 30 min	++
Methyl-β-cyclodextrin (MβCD)	Cholesterol decrease	20 mM, 10 min	++
Cholesterol (EtOH)	Cholesterol increase	30 μM, 2 h	+
Lanosterol (EtOH)	Lanosterol increase	30 μM, 2 h	+
4-cholesten-3-one (EtOH)	4-cholesten-3-one increase	30 μM, 2 h	-
25-Hydroxycholesterol	Cholesterol activation	20 μM, 4 h	+
Lovastatin	Cholesterol synthesis inhibitor	5 μM, 4 h	–
U18666A	Cholesterol trafficking inhibitor	5 μM, 4 h	–
Nodocazole	Blocks microtubuli polymerization	1 μM, 4 h	–
Brefeldin A	ER to golgi transport inhibition	20 μM, 4 h	–
Forskolin	Adenylyl cyclase activation	100 μM, 1 h	–
H89	Protein kinase A inhibition	20 μM, 1 h	–
Phorbol 12-myristate 13-acetate	Protein kinase C activation	100 μM, 1 h	–
Lysophosphatidic acid	Rho kinase activation	10 μM, 30 min	–
Y27632	Rho kinase inhibition	100 μM, 1 h	–
Wortmannin	Phosphoinositide 3-kinase inhibition	100 μM, 1 h	–
U73122	Phospholipase C inhibition	100 μM, 1 h	–
Sucrose	Osmotic stress	0.45 M, 10 min	++

presence of sucrose (450 mM) or eflucimibe (iACAT) (0.5 μM, 1 h). The membrane proteins were analyzed by SDS-PAGE and immunoblotting (Figure 6B). The migration pattern of ACAT in SDS-PAGE was markedly affected by the temperature at which the samples were incubated prior to gel electrophoresis. Heating the samples at 40°C, 70°C or 95°C for 10 min in SDS loading buffer revealed substantial differences in their electrophoretic mobility (Figure 6B). Monomeric AcGFP-tagged ACAT was running at a ~85 kDa species which was again slightly lower than its calculated molecular weight (~94 kDa). In addition to this species, a lower molecular ~70 kDa form appeared at 40°C and disappeared at higher temperatures (70°C and higher). At 95°C, the intensity of the monomeric ~85 kDa ACAT species was decreasing while at the same time higher molecular ACAT dimers and oligomers appeared. However, when compared with untreated cells, neither eflucimibe nor sucrose led to substantial alterations in the gel-mobility of ACAT.

Finally, the electrophoretic mobility of ACAT was explored under crosslinking conditions. AC29-ACAT cells were incubated in the absence or presence of sucrose (450 mM) or eflucimibe (iACAT) (0.5 μM) for 1 h. Then, the membrane-permeable aminoreactive crosslinker disuccinimidyl suberate (DSS) was added to the cells at increasing concentrations (0.01, 0.1, 1 mM) for 30 min at 37°C. The cells were washed with PBS, homogenized by sonication, and centrifuged by 30,000 g for 30 min (4°C). The pelleted proteins were dissolved in SDS loading buffer and were treated for 10 min at 70°C prior to gel loading, separation by SDS-PAGE, and immunodetection using anti-ACAT/SOAT antibody. To demonstrate the successful crosslinking with DSS, the remaining proteins of the SDS gel were stained by Coomassie. As shown in Figure 6C (lower panel), DSS at concentrations of 1 mM produced high molecular protein aggregates that partly remained in the stacking gel. In the presence of increasing concentrations of the crosslinker DSS, the intensity of the monomeric anti-ACAT species was decreasing while at the same time higher molecular anti-ACAT species (dimers and oligomers) appeared as expected (Figure 6C). However, even after chemical crosslinking, ACAT translocation was not associated with changes in the electrophoretic mobility of the protein. In addition, no signs of proteolysis during the translocation process of ACAT were observed.

Translocated ACAT can esterify cholesterol efficiently

Is ACAT associated with a change or loss of its enzymatic activity in its vesicular environment? To address this question, we used the fluorescent cholesterol reporter DChol and established an *in vitro* assay to measure the activity of ACAT. When both substrates, DChol (10 μM) and oleoyl-CoA (0.8–64 μM) were added to microsomes from AC29-ACAT cells, an esterification of DChol was clearly observed (Figure 7A). Increasing the substrate concentration of oleoyl-CoA resulted in increasing rates of DChol esterification. At high concentrations of oleoyl-CoA, saturation of the enzyme was observed as expected (Figure 7B). Using this assay, the activity of vesicular *versus* non-vesicular ACAT was compared.

10.3389/fmolb.2023.1258799

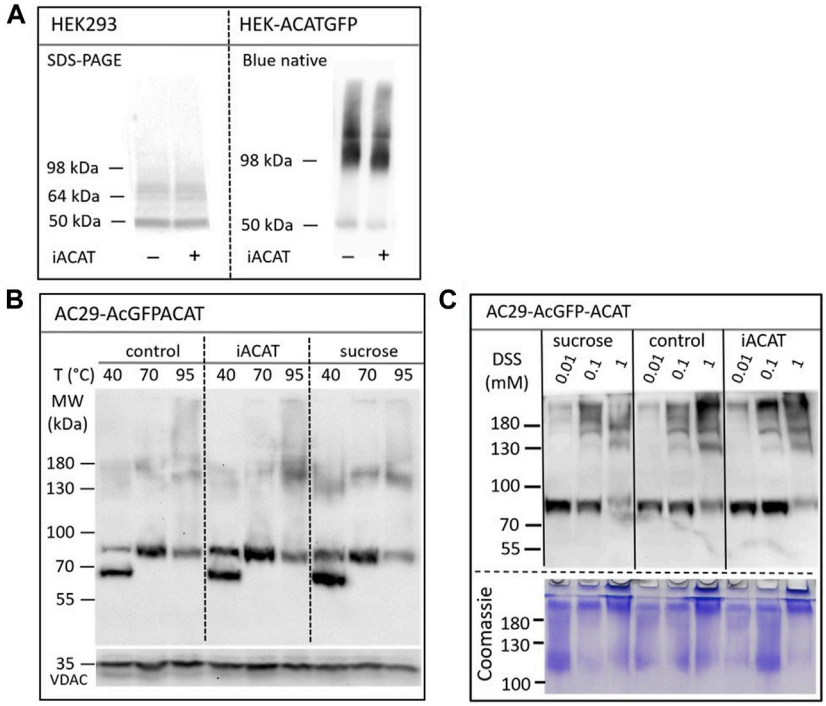

FIGURE 6
Analysis of the electrophoretic mobility of ACAT in dependence of the translocation inducers eflucimibe (iACAT) and/or sucrose. **(A)** HEK293 cells transfected or not transfected with ACATGFP were incubated for 1 h in the presence or absence of eflucimibe (0.5 μM). Membranes of these cells were prepared and the proteins were separated by denaturing SDS-PAGE or by non-denaturing Blue native gel electrophoresis, followed by immunoblotting. **(B)** AC29-ACAT cells were incubated in the absence (control) or presence of sucrose or eflucimibe (iACAT) for 1 h. The cells were homogenized and the membrane proteins were analyzed by SDS-PAGE and immunoblotting. Prior to gel electrophoresis, samples were heated for 10 min at either 40°C, 70°C or 95°C in SDS loading buffer. Immunodetection of ACAT was performed using anti-ACAT/SOAT antibody, while VDAC (~35 kDa) was used as a loading control. **(C)** AC29-ACAT cells were treated or not treated (control) with sucrose or eflucimibe (iACAT) for 1 h. Then, the membrane-permeable aminoreactive crosslinker disuccinimidyl suberate (DSS) was added to the cells at increasing concentrations (0.01, 0.1, 1 mM) for 30 min at 37°C. After washing-off the crosslinker, the cells were homogenized and the membrane proteins were analyzed by SDS-PAGE and immunoblotting using anti-ACAT/SOAT antibody. The results were confirmed in a second experiment.

Of course, an ACAT inhibitor as the stimulus for ACAT translocation could not be employed in these experiments. For this purpose, hyperosmotic sucrose treatment of cells was used as the stimulus to induce the translocation of ACAT. The experiments were performed in AC29-ACAT cells as well as in HeLa cells endogenously expressing ACAT. The cells were incubated for 1 h in the absence (control) or presence of sucrose (450 mM in DMEM medium). The ACAT translocation in sucrose treated cells was confirmed by microscopical inspection. All cells were harvested by a cell scraper and their microsomes were prepared. The ACAT activities of these microsomes were measured by the *in vitro* assay mentioned above. Following lipid extraction and separation by TLC, the DChol and DChol-oleate bands were quantified by fluorimetry. The band intensities of DChol, DChol-ester as well as the ratios of DChol-ester to DChol were calculated (Table 3). The data are graphically displayed in Figure 8, with the control cell data set to 100%. In microsomes from HeLa cells, nearly 5-fold lower DChol-ester amounts were found as compared with microsomes from AC29-ACAT cells (Table 3). This is certainly due to the higher expression level in AC29-ACAT cells. More importantly, it was found that the ACAT activities in microsomes from both sucrose treated cells were at least as high as those obtained in microsomes from untreated cells. From this, it can be concluded that ACAT, which is translocated into vesicles in response to osmotic stress, is fully activatable when sufficient substrate is available.

Discussion

This study was initiated by the incidental observation that commonly used ACAT inhibitors induce a fast (within minutes) intracellular translocation of ACAT from the extensive network of the endoplasmic reticulum into a vesicular compartment. This occurred in all cells studied so far. In the process, we also discovered that a number of other substances or treatments can induce such a ACAT translocation, e.g., cholesterol or lanosterol at concentrations > 30 μM, 25-hydroxycholesterol, and certain stressors such as osmotic stress induced by sucrose, exposition of the cells to lower temperatures or cultivation of the cells at maximum density. The question arises how a treatment with cholesterol amounts > 30 μM relates to the free cholesterol in culture medium/FCS and in cells. According to our measurements, HEK-ACAT cells grown on 35-mm dishes (~10^6 cells) possess ~7 nmol of free cholesterol and were cultured in medium/10% FCS with 28 nmol of free cholesterol. So, at least 60 nmol of cholesterol was added to the cells, i.e., nearly 10 times

10.3389/fmolb.2023.1258799

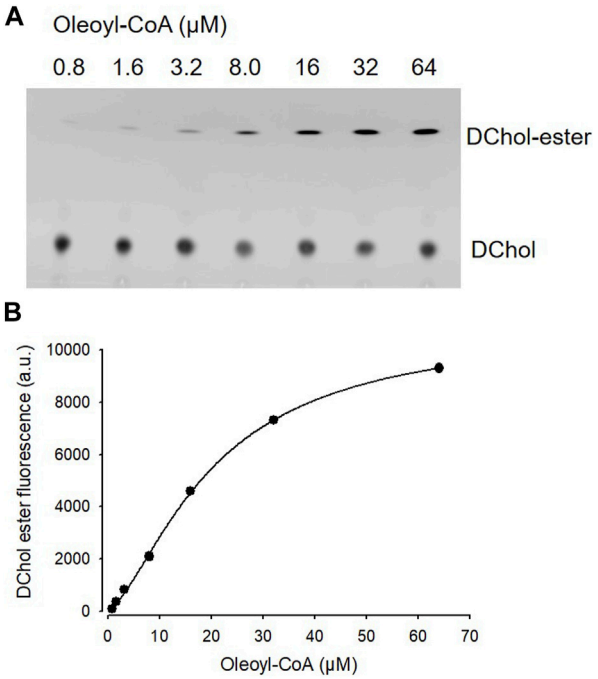

FIGURE 7
ACAT activity assay in microsomes. **(A)** Microsomes prepared from AC29-ACAT cells (2 × 10^6 cells) were resuspended in 300 μL assay buffer (20 mM Hepes, pH 6.8, 2 M KCl). After addition of 1 μL DChol-MβCD (3 mM stock), the assay was mixed and incubated for 5 min at 25°C. The esterification reaction was initiated by addition of 1 μL oleoyl-CoA (final 0.8–64 μM from increasing stock solutions). After incubation for 2 h at 37°C, the lipids were extracted and separated by TLC on silica gel G plates using petrolether:diethylether: acetic acid (8:2:1, v/v/v) as the solvent system. **(B)** The DChol ester bands were quantified by fluorimetry. The data were best fit by a 4-parameter logistic function yielding an EC_{50} of 20.1 μM for oleoyl-CoA (other parameters: max 10.877, min 97.3, slope 1.5). Data from one experiment performed in triplicate.

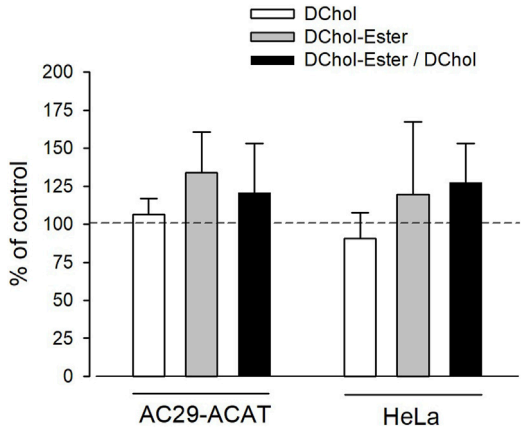

FIGURE 8
Analysis of sucrose-induced ACAT translocation on the activity of ACAT. AC29-ACAT and HeLa cells were cultivated in 6 cm dishes and were incubated in the absence (control) of presence of sucrose (450 mM) for 1 h at 37°C. The cells were harvested, lysed by sonication and subjected to microsomal preparation. The microsomes were resuspended in 300 μL assay buffer (20 mM Hepes, pH 6.8, 2 M KCl). After addition of 1 μL DChol-MβCD (final 10 μM), the assay was mixed and incubated for 5 min at 25°C. The esterification reaction was initiated by addition of 1 μL oleoyl-CoA (final 20 μM). After incubation for 2 h at 37°C the lipids were extracted and separated by TLC. DChol and DChol ester bands were quantified by fluorimetry. The band intensities of DChol (white bars), DChol-ester (grey bars) as well as the ratios of DChol-ester to DChol (black bars) were calculated. The data of the untreated cells were set to 100%. The respective values of the sucrose-treated cells are graphically shown as a percentage of this (±SD, n = 3) (data in Table 3). The differences between control and sucrose treatment remained below the significance level in case of both DChol and DChol-ester.

TABLE 3 ACAT activity in microsomes from AC29-ACAT and HeLa cells treated or not treated with sucrose (450 mM for 1 h). The cells were harvested, lysed by sonication and microsomes were prepared as described. The ACAT activity in these microsomes was measured using the substrates DChol and oleoyl-CoA. After extraction and separation of the lipids by TLC, the DChol and DChol ester bands were quantified by fluorimetry. The fluorescence intensities (a.u.) are given as means ± SD obtained from three experiments.

Cell	Parameter	Control	Sucrose
AC29-ACAT	DChol	19,994 ± 1,344	22,703 ± 1,477
	DChol-ester	3,523 ± 1,176	4,702 ± 1,622
	DChol-ester/DChol	0.177 ± 0.058	0.205 ± 0.055
HeLa	DChol	21,756 ± 5,125	19,115 ± 1,113
	DChol-ester	951 ± 505	1027 ± 340
	DChol-ester/DChol	0.042 ± 0.01	0.053 ± 0.015

more cholesterol than the cells possess. However, the calculations also show that cells cultured in medium with 20% FCS would be exposed to cholesterol concentrations at which ACAT translocations could be induced. It is unclear whether under pathological conditions, e.g., atherosclerosis, such high cholesterol concentrations are reached. While the majority of ACAT vesicles in the present study showed no clear assignment to a defined compartment, a small population of these vesicles was located in close proximity to peroxisomes. This is of potential interest because membrane contacts between peroxisomes and lysosomes represent an important transport pathway for LDL-derived cholesterol. Disruption of these contacts induces massive cholesterol accumulation in lysosomes, as observed in fibroblasts from patients with different types of peroxisomal disorders (Chu et al., 2015). Peroxisomes play a central role in the cellular lipid metabolism. For example, the β-oxidation of fatty acids, the pre-squalene segment of the cholesterol biosynthesis and the formation of bile acids take place in this organelle (Charles et al., 2020). Principally, at such peroxisomal contact sites, ACAT could have access to LDL-derived cholesterol and to its co-substrate acyl-CoA, which can possibly be provided by acyl-CoA synthetases localized to the surface of peroxisomes (Chornyi et al., 2020). However, this issue requires further investigation.

Of particular importance is our finding that translocation of ACAT from the extensive ER network into vesicular structures is a reversible process that under certain conditions can even be triggered twice in succession on cells, for example, after application and removal of the ACAT inhibitor eflucimibe. Remarkably, oleic acid was able to greatly accelerate the re-

translocation of ACAT from the vesicles back to the ER. Considering that oleic acid in its activated form (oleoyl-CoA) is a preferred fatty acid substrate of ACAT (Chang et al., 2010), it could be speculated that this translocation process might be of physiological relevance. Treatment of cells with oleic acid is commonly used to induce the formation of lipid droplets, i.e., the storage of lipids. The development of lipid droplets requires ACAT whose activity depends on the availability of both, cholesterol and long-chain fatty acyl-CoA. The latter are produced by acyl-CoA synthetases localised on peroxisomal, ER and mitochondrial outer membranes (Fuellekrug et al., 2012). The re-translocation of ACAT from vesicles into the ER network in response to oleic acid, i.e., under lipid storage conditions appears reasonable in view of the following aspect. The extensive network of the ER in the cell, in which ACAT is evenly distributed under normal physiological conditions, provides an enormous surface area and ensures that cholesterol can be efficiently used as substrate. ACAT immediately esterifies ´active` cholesterol molecules that flow from the plasma membrane into this giant ER compartment using Aster transfer proteins (Sandhu et al., 2018; Naito et al., 2019). Subsequently, the esters are deposited into lipid droplets. This process serves to store energy and also counteracts the accumulation of free cholesterol, that is toxic to the cell. With an adequate supply of cholesterol and oleoyl-CoA, the distribution of ACAT in the ER network seems to be appropriate and well adapted. But what could be the benefit of localising ACAT in vesicles? A regulatory function would be obvious. In particular, this way the enzyme would not be exposed to the non-vesicular influx of cholesterol from the plasma membrane, which is a major pathway of cholesterol entry into the cell (Maxfield and Tabas, 2005; Ikonen, 2008). The availability and accessibility of ACAT to its substrates could be completely different in these vesicular structures than within the ER network. It is possible that the enzyme gains access to other vesicular transport routes within the cell. At this point, it is also worth remembering that ACAT has two different tasks to fulfil in cholesterol metabolism. It must provide cholesterol esters not only for storage in lipid droplets but also for the formation of lipoproteins. How these two so different functions of the enzyme are regulated is still completely unclear. Regulation of the enzymatic activity through a differential localization would be a conceivable scenario. It is also possible that the translocation of ACAT into vesicles is associated with the strengthening of ER-mitochondria connectivity in response to ACAT inhibition as recently reported (Harned et al., 2023).

In addition to peroxisomes, we observed a weak colocalization of ACAT vesicles with mitochondria and lysosomes. The association of both organelles with ACAT vesicles was higher in cell regions where larger ACAT vesicles were frequently located. In macrophages or macrophage-derived cell lines, the localization of ACAT1 in vesicular structures and the association of these vesicles with various organelles have already been observed by others (Khelef et al., 2000; Li and Pownall, 2000; Lei et al., 2010; Sakashita et al., 2010; Kamikawa et al., 2014). For example, a fraction of ACAT1 immunoreactivity was present in ER-derived, perinuclear structures near the *trans*-Golgi network and the endocytic recycling compartment (Khelef et al., 2000). In a mouse macrophage cell line, High Density Lipoprotein 2 was reported to induce ACAT translocation from perinuclear sites to vesicular structures at the cell periphery and this process was sensitive to Brefeldin, an inhibitor of protein trafficking from ER to Golgi (Li and Pownall, 2000). Interestingly, ACAT1 positive vesicles have also been observed following cholesterol loading (Lei et al., 2010; Sakashita et al., 2010; Kamikawa et al., 2014). Using LAMP2 as marker protein ACAT1 was found to be associated with late endosomes/lysosomes and this colocalization increased after cholesterol loading of the cells (Kamikawa et al., 2014). However, in another study, the association of ACAT1 vesicles with late endosomes/lysosomes was observed only after cholesterol enrichment of cells (Lei et al., 2010). In isolated ER-derived vesicles, Sakashita et al. (2010) detected an increased ACAT activity and speculated in this regard on a mechanism by which ACAT might upregulate its enzymatic activity without having to produce more protein. Actually, we also observed here the formation of ACAT containing vesicles in response to cholesterol. Moreover, 25-hydroxycholesterol, which is known to activate the esterification of cholesterol, was able to induce the translocation of ACAT (Underwood et al., 1998; Du et al., 2004). This suggests that vesicular ACAT can be associated with enhanced enzymatic activity. Interestingly, ACAT translocation also spontaneously occurred when cells approached confluency. Cell growth appears to be correlated with the esterification of cholesterol (Dessi et al., 1997; Batetta et al., 2003). In endothelial cells, both cholesterol and cholesteryl ester increased markedly as cells reached confluency (Corvera et al., 2000). The same was observed for CHO cells (Liu et al., 2004; Takahashi et al., 2007). Thus, ACAT activity appears to be upregulated with increasing cell density, again suggesting that the enzyme functions very efficiently in its vesicular environment.

Despite some efforts, we failed to detect the translocation process of ACAT in cells endogenously expressing the enzyme (e.g., in HeLa cells) by immunocytochemistry using the commercially available antibodies, although these antibodies were suitable for the detection of ACAT in immunoblots. The question arises whether and how overexpression of ACAT affects the translocation of ACAT. To address this issue, the number and size of ACAT vesicles was analyzed in HEK-ACAT cells expressing the enzyme at different levels. After induction with eflucimibe, the mean size of ACAT vesicles increased with the expression of the enzyme, while the highest number of vesicles appeared at intermediate ACAT expression. In addition, the level of ACAT expression was found to increase the probability of triggering ACAT translocation, ranging from ~70% in cells with low ACAT expression to 95% in cells with higher expression. Thus, it appears that sufficient numbers of ACAT molecules are required to clearly visualize this translocation process microscopically. According to biochemical and structural data, ACAT was proposed to form tetramers (Rogers et al., 2012; Rogers et al., 2015; Guan et al., 2020; Qian et al., 2020). Thus, it is reasonable to speculate that ACAT translocation could be related to dimerization/oligomerization of the protein. Assuming that ACAT dimers/tetramers are in equilibrium with higher-order oligomers in the ER membrane, increased expression of ACAT should also enhance the formation of oligomeric complexes. So, it cannot be excluded that higher-order oligomers of ACAT can somehow contribute to vesicle formation in ACAT overexpressing cells. Although we did detect some higher molecular weight ACAT complexes in native blue gels and in SDS-PAGE after cross-linking, ACAT translocation was not associated with significant changes in protein electrophoretic mobility.

There is some evidence that at least one other unknown protein is required for ACAT translocation since the protein synthesis inhibitor cycloheximide was able to block this translocation process. The cycloheximide effect is interesting because it refers to earlier

observations that remained unexplained. ACAT activity was found to be enhanced by cycloheximide treatment which lead to the conclusion that there is a short-lived protein inhibitor of ACAT-mediated cholesterol esterification (Chang et al., 1986; Tabas and Boykow, 1987). It was also reported that cycloheximide (and other translation inhibitors) are able to induce the formation of cholesterol ester-rich lipid droplets (Suzuki et al., 2012), a finding which could be confirmed here for HeLa cells. The results of our study may provide a simple explanation for this observation, because cycloheximide-induced prevention of ACAT translocation could lead to persistent esterification of plasma membrane cholesterol and thus to an increased lipid droplet formation. As mentioned above, this non-vesicular cholesterol influx into the ER is regarded as the major pathway of cholesterol entry into the cell. The molecular machinery that can be induced by cycloheximide appears to be complex. So, it was recently reported that treatment of HeLa cells with cycloheximide and other translation elongation inhibitors are able to activate the MondoA pathway (Wilde et al., 2020). As a member of the MLX family of glucose-sensing transcription factors, MondoA is not only a key regulator of the energy metabolism (Ke et al., 2021) but also plays an important role in the regulation of cholesterol/steroid metabolism (Mejhert et al., 2020; Weger et al., 2020).

ACAT enzymes are crucial components of cholesterol metabolism, and inhibition of their activity has great therapeutic potential, e.g., against hyperlipidemia, atherosclerosis, Alzheimer´s disease, Niemann Pick C disease, viral activity, and tumor growth (Giovannoni et al., 2003; Llaverias et al., 2003; Hutter-Paier et al., 2004; Huttunen et al., 2007; Yue et al., 2014; Yang et al., 2016; Bandyopadhyay et al., 2017; Li et al., 2018; Chang et al., 2021; Ren et al., 2021; Rogers et al., 2022; Wing et al., 2023). For example, avasimibe, one of the most widely used ACAT inhibitors and a potent inducer of ACAT translocation in this study, has recently emerged as a promising anti-tumor compound (Yang et al., 2016; Xiong et al., 2021; Websdale et al., 2022; Zhu et al., 2022). We show here that ACAT inhibition is associated with rapid changes of the intracellular distribution of ACAT. However, future studies are needed to confirm these observations, particularly in cells endogenously expressing ACAT/SOAT.

Materials and methods

Materials

The substances were from the following suppliers: bovine serum albumin (BSA, fraction V), Biomol (Germany); lipofectamine 2000, ThermoFisher; Rotifect Plus, Carl Roth; SAN 58035, Novartis; eflucimibe (=F12511), gift from Institute de Recherche Pierre Fabry (France); tamoxifen, avasimibe, auraptene, piperine, Merck; T4 DNA Polymerase, Phusion High-fidelity DNA polymerase (PCR), DNA ligase, and all restriction enzymes, New England Biolabs (NEB); Mowiol 4–88, calbiochem (Bad Soden, Germany); disuccinimidyl suberate (DSS), Sigma; Mitotracker orange CMTMRos, lysotracker Red, ThermoFisher; wheat germ agglutinin, Texas Red-X Conjugate (WGA-TR), Bodipy 493/503, ThermoFisher; i-block (Tropix, Applied Biosystems). Antibodies: anti-calnexin, Santa Cruz, #23954; anti-ACAT/SOAT, Santa-Cruz, #sc69836; anti-mouse IgGκ-BP, Santa Cruz, #sc516102 (HRP-conjugated); anti-mouse-Cy3, Sigma, #C2181; anti-VDAC, Santa Cruz, #390996; anti-Golgin-97, ThermoFisher, #A21270; anti-sec31A, BD Transduction laboratories, #612350.

All other substances, unless otherwise stated, were from Merck (Darmstadt, Germany).

Preparation of oleic acid-BSA, DChol, and sterol-MβCD complexes

Oleic acid (OA) (400 μM) was dissolved in ethanol and evaporated under nitrogen to a thin film. Then, 10% BSA in phosphate-buffered saline (PBS) at 45°C was added to the tube to obtain the desired oleic acid-BSA complex. After the fatty acid was completely dissolved, the solution was cooled, filtered, and stored in aliquots at 4°C. DChol was synthesized in our group (Wiegand et al., 2003) using a modified protocol of Kawasaki et al. (1982). In brief, 6-ketocholestanol mixed with dansyl hydrazine (5x excess) in dried methanol was stirred for 6 h at 65°C with catalytic amounts of concentrated HCl. Methanol was evaporated, and the reaction product was separated by silica gel column chromatography and an additional thin layer chromatography (TLC), both in chloroform-ethanol (95:5, vol/vol). A second separation with the same running medium was performed by TLC using preparative silica gel. The purified substance (DChol) was analyzed by field decomposition mass spectrometry and was identified as a peak with MW 649.5 (overall yield ~35%, purity >95%). Inclusion complexes of sterols and MβCD were performed as described (Wiegand et al., 2003). For preparation of DChol-MβCD, the steroid (final concentration of 3 mM) was added to an aqueous solution of MβCD (30 mM) in a 2 mL tube. The mixture was overlaid with N_2 and was vortexed for 24 h at 30°C. The solution was centrifuged to remove insoluble material before use.

Expression plasmids and cloning

The cDNA encoding human ACAT1 was obtained from RZPD (Berlin, Germany) and was amplified by PCR using the primers 1_for (5′-GCATTTGTACAAGCCCGGCGTGGGTGAAGAGAA GATGTCTCTA-3′) and 2_rev (5′-GCATTGCGGCCGCCTAAA ACACGTAACGACAAGTCCAG-3′), digested with BsrGI and NotI (~1.7 kb fragment). To obtain the plasmid pcDNA5/FRT-GFP, pEGFP-N3 (Clontech) was cut with NotI, blunted with T4 Polymerase and further digested with NheI. The resulting ~ 700 bp fragment was ligated with pcDNA5/FRT cut with NheI + EcoRV. To construct pcDNA5/FRT-GFP-ACAT1, pcDNA5/FRT-GFP restricted with BsrGI and NotI was ligated with the PCR product of hACAT1 that has been digested with BsrG1 + NotI. The plasmid pAcGFP-ACAT1 was a ligation product of the vector pcDNA5/FRT-GFP-ACAT1, digested with BsrGI, blunted with T4 DNA polymerase, cut with NheI, and the insert encoding AcGFP that was isolated from pAc-GFP-Sec61beta (from Tom Rapoport, Addgene #15108) restricted with BglII, blunted with T4 DNA polymerase, and digested with NheI. To create pcDNA-AcGFP-ACAT1, the vector pfmOTRf (Gimpl et al., 1997) cut with HindIII, blunted with T4 DNA polymerase, and digested with XhoI was ligated with the AcGFP encoding insert isolated from pAcGFP-

ACAT1, cut with NheI, blunted with T4 DNA polymerase, and restricted with XhoI. To obtain pcDNA5/FRT-BTBhACAT1, the sequence encoding GFP was removed and substituted by the BTB motif. The vector pcDNA/FRT-GFPhACAT1 was digested with BsrGI and NheI and was ligated with an adapter cDNA encoding the BTB-motif. The adapter was created by annealing the two oligonucleotides BTB_1 (5′-CTAGCACCATGGGATGGAGAT ACTACGAGAGCTCCCTGGAG CCCTACCCTGACGGCAT-3′) and BTB_2 (5′-GTACATGCCGTCAGGGTAGGG CTCCAGGG AGCTCTCGTAGTATCTCCATCCCATGGTG-3′). To create the plasmid pDsRed-Peroxi, the calreticulin signal sequence of pDsRed2-ER (Clontech) was removed by cleavage with NheI and BglII. The vector was ligated with the insert obtained by PCR using the template pDsRed2-ER, the oligonucleotides SKL_for (5′-GCC GGCTAGCATGGCCTCCTCCGAGAAC-3′) and SKL_rev (5′-GGCAGATCTACAGCTTGGACTTGTACGATCTCAGGAACA GGTGGTGGCGGCC-3′), followed by digestion with NheI and BglII.

Cell culture, transfection, and membrane preparation

HEK293, HepG2, Saos2, COS-7 and HeLa cells were cultivated in DMEM plus 10% FCS. CHO-K1 and AC29 cells were grown in DMEM/Ham's F12 medium with 10% FCS. Transfections were performed with lipofectamine 2000 or Rotifect Plus according to the instructions of the supplier. To prepare membranes, the cells were harvested by centrifugation at 1,000 g. Then, the cells were resuspended in hypotonic lysis buffer (20 mM Hepes, 7.4, 5 mM $MgCl_2$) and were homogenized by a Potter-Elvehjem Homogenizer or by sonication (Branson sonifier). In some experiments, cell debris and nuclei were removed by low-speed centrifugation (5,000 rpm). The membranes were pelleted for 30 min at 31,000 g (4°C), and resuspended in lysis buffer or in an appropriate working buffer. Protein was determined by the Bradford assay (Roti-Quant) using bovine serum albumin as standard.

Lipid extraction and analysis

All lipid extractions were performed by the method of Bligh and Dyer (Bligh and Dyer, 1959), slightly modified as described (Maiwald et al., 2017). To measure the esterification of DChol, the cells were grown on Petri dishes for various times with culture medium/10% FCS containing 7.5 µM DChol-MβCD. After washing-off the cholesterol donor, the cells were incubated in culture medium at 37°C for different times in the presence or absence of the indicated ACAT inhibitor (e.g., eflucimibe). The cells were harvested by scraping and their lipids were extracted. The lipids were dissolved in chloroform, separated by silica gel thin layer chromatography (TLC) using heptane/diethyl ether/methanol/acidic acid (80:35:3:2, vol%) as mobile phase. The fluorescence was detected under UV and was imaged with a CCD camera (UVP ChemStudio, Analytic-Jena). Quantification of the data were performed by the software VisionWorks or ImageJ (Fuji version). Cholesterol was assayed spectrophotometrically using R-Biopharm kit (Darmstadt, Germany) performed in a microscale dimension.

Fluorescence microscopy and imaging

In most experiments, cells grown on Petri dishes were transferred to 3 cm glass-bottom dishes (MatTek, United States) for imaging. In some experiments, cells were grown on glass coverslips in Petri dishes. These coverslips were placed in an imaging chamber (Life Imaging Services, Switzerland), which was inserted into an adapter on the microscope stage and temperature controlled with a Peltier device. Cells were imaged using a Zeiss Axiovert 100 with a 100x/1.3 Fluar objective and a cooled MicroMax CCD camera (Princeton Instruments, Trenton, NJ) driven by a MetaView Imaging system (Universal Imaging Corporation), a Zeiss Axiovert Observer Z.1 (63x/1.43 objective, with Apoptome mode, camera Axiocam 503 mono) driven by ZEN software, or a Leica TCSSP confocal microscope. Time-lapse imaging was performed using either a monochromator (Polychrome II, TILL Photonics, Germany), a LED source (Colibri 7, Zeiss), or lasers (488, 561, 647 nm, Leica) for excitation.

In some experiments, cells were labelled with DChol or with the fatty acid probe Bodipy-C12-568. After a washing step, the fluorescent lipid droplets were counted. The images were thresholded, binarized and processed for particle counting using ImageJ software (NIH). In living cells, fluorescence imaging was performed with imaging buffer (10 mM Hepes, pH 7.4, 145 mM NaCl, 4.5 mM KCl, 1.2 mM $MgCl_2$, 1.2 mM $CaCl_2$) or in Hepes-buffered (10 mM, pH 7.4) culture medium (without phenol-red) with or without 10% FCS.

To study the effect of cycloheximide on the development of lipid droplets, HEK293 or HeLa cells cultivated in 3 cm glass-bottom dishes were incubated with cycloheximide (20 µM) for 30 min up to 12 h at 37°C. Thereafter, Bodipy 493/503 (4 µM) was added for 30 min. After a washing step, the cells were imaged and droplets were counted as described above.

To analyse the kinetic and reversibility of the translocation process of ACAT, the cells were cultivated in a temperature controlled microchamber on the Leica or Zeiss setup. We always used 30°C for live cell microscopy because focus drift problems often occurred at 37°C in our microscopy setup. The translocation of ACAT was initiated by eflucimibe (0.5 µM). Images were captured each 20 s. The vesiculation process was quantified by using the particle counting module of ImageJ (NIH). Images were background subtracted, stacked, and particles were counted. After washing-off eflucimibe the reversibility of the vesiculation was initiated by addition of BSA (10%) or BSA-bound oleic acid (400 µM OA in 10% BSA).

Some substances used in this study were dissolved in ethanol or DMSO before their dilution in aqueous buffers. In control experiments with cells to which appropriate amounts of these solvents were added, no effects on the translocation of ACAT were detected.

Sigmaplot 8.0 was used to fit the data according to the appropriate functions and to draw the graphs. Colocalization of fluorescent structures was calculated using the Pearson correlation coefficient (ImageJ, NIH). Student's t-test was used to calculate the statistical significance of data.

Gel electrophoresis, Western blot and immunocytochemistry

In most cases, proteins of cellular membranes were separated by SDS-PAGE. Prior to gel electrophoresis the samples were heated for

10 min either at 40°C, 70°C or 95°C in SDS loading buffer. In some experiments, the non-denaturing Blue native gel electrophoresis was performed according to Schägger (Schaegger and von Jagow, 1991). The proteins that have been separated by gel electrophoresis, were transferred to nitrocellulose and were subjected to immunoblot analysis. After a blocking step with i-Block for 1 h, the immunodetection of ACAT was performed using anti-ACAT/SOAT antibody (1:200 in i-Block) and anti-mouse IgGκ-BP (1:1000 in i-Block, HRP conjugated) as the secondary antibody. Alternatively, anti-mouse-IgG binding protein (HRP conjugated) was used as the antibody detecting reagent. Anti-VDAC (1:100) was used as a loading control. The immunoblot was developed using Western blotting Luminol Reagent (sc-2048).

The cells that were processed for immunocytochemistry were grown on an 18 mm coverslip placed either in a six well plate or in a microchamber. The cells were fixed with 3.7% paraformaldehyde in PBS for 15 min at 25°C. After washing-off the fixation reagent, the cells were incubated with the appropriate antibody, i.e., anti-calnexin (mouse) (1:100), anti-Golgin (1:50), or anti-Sec31 (1:50). As the secondary antibody anti-mouse-Cy3 (1:1000 in PBS/5% FCS) was applied. All antibodies were diluted in PBS/5% FCS. The cells were either subsequently imaged in PBS or were mounted in Mowiol 4–88 before imaging.

Crosslinking studies

AC29-ACAT cells were used to analyse the electrophoretic mobility of ACAT in dependence of ACAT inhibition and sucrose. The cells grown in six-well plates were treated or not treated with sucrose or eflucimibe for 1 h. Then, the membrane-permeable aminoreactive crosslinker disuccinimidyl suberate (DSS) (dissolved in DMSO) was added to the cells at increasing concentrations (0.01, 0.1, 1 mM) for 30 min at 37°C. After washing-off the crosslinker with PBS, the cells were harvested by scraping and were immediately homogenized in PBS by sonication (7 s, 40%, using HTU soni 130, Heinemann, Germany). After centrifugation (for 1 h at 32,000 g) the homogenate pellet was resuspended in SDS loading buffer. Proteins were heated at 70°C for 10 min and separated by SDS-PAGE, followed by immunoblot analysis with anti-ACAT/SOAT antibody as described above.

ACAT activity assays

In cells, the cholesterol esterification was measured using DChol as substrate. Cells grown on Petri dishes were labelled with DChol-MβCD (7 μM) or (as control) with Chol-MβCD (7 μM) in culture medium/10% FCS at 37°C in the absence or presence of an ACAT inhibitor (iACAT) (e.g., eflucimibe at 0.4 μg/mL). The medium was removed and the cells were washed twice with PBS. Then, the cells were harvested by scraping and their lipids were extracted as described above.

In microsomes, the assay was performed as follows. AC29-ACAT cells grown on 10 cm Petri dishes were washed with PBS, were then harvested by a cell scraper and centrifuged for 5 min at 500 g. The cell pellet (~1×10^7 cells) was resuspended in 500 μL PBS, sonicated (for 4 s at 40% intensity using a Branson sonifier), and was then centrifuged for 1 h at 32,000 g. The pellets were frozen in aliquots at −70°C. To measure the ACAT activity, the membrane pellet (2×10^6 cells) was resuspended in 300 μL assay buffer (20 mM Hepes, pH 6.8, 2 M KCl). After addition of 1 μL DChol-MβCD (3 mM stock), the assay was mixed and incubated for 5 min at 25°C. The esterification reaction was initiated by addition of 1 μL oleoyl-CoA (final 0.8–64 μM from increasing stock solutions). After incubation for 2 h at 37°C the lipids were extracted, and were separated by TLC on silica gel plates using petrolether: diethylether:acetic acid (8:2:1, vol%) as the solvent system. DChol and DChol ester bands were quantified by fluorimetry (see above).

Data availability statement

The original contributions presented in the study are included in the article/Supplementary Materials, further inquiries can be directed to the corresponding author.

Author contributions

AS: Methodology, Software, Writing–original draft. LA: Methodology, Writing–review and editing. GG: Conceptualization, Funding acquisition, Investigation, Project administration, Supervision, Writing–original draft, Writing–review and editing.

Funding

The author(s) declare that no financial support was received for the research, authorship, and/or publication of this article.

Acknowledgments

We thank Larisa Cristea and Conny Trossen for their help in this research project. AC29 cells were kindly provided by T. Y. Chang (Dartmouth, United States).

Conflict of interest

The authors declare that the research was conducted in the absence of any commercial or financial relationships that could be construed as a potential conflict of interest.

Publisher's note

Supplementary material

The Supplementary Material for this article can be found online at: https://www.frontiersin.org/articles/10.3389/fmolb.2023.1258799/full#supplementary-material

SUPPLEMENTARY FIGURE S1
Most DChol containing droplets are associated with the endoplasmic reticulum. COS-ACAT cells labeled with DChol-MβCD (10 μM) for 30 min were washed and further incubated for 7 h. The distribution of ACAT-GFP (green) and DChol/ester (red) was imaged. Most DChol containing droplets are closely associated with the ER as shown for the droplet marked with arrowhead. Data from a representative experiment (n = 2) (bar, 3 μm) (Image J processing, using flattened background).

SUPPLEMENTARY FIGURE S2
ACAT translocation in HEK cells transfected with AcGFPACAT. HEK cells were stably transfected with AcGFP-ACAT. **(A,B)** show the same cells before **(A)** and after **(B)** administration of iACAT for 10 min. Image C shows another cell ~30 min after application of iACAT. Data from a representative experiment (n = 3) (Bars, 5 μm).

SUPPLEMENTARY FIGURE S3
Colocalization of ACAT vesicles with organelle-specific markers. HEK-ACAT cells were treated with eflucimibe for 1 h. Then, living cells were incubated with lysotracker Red (50 nM, 10 min) **(A)**, with wheat germ agglutinin, Texas Red-X Conjugate (WGA-TR) (10 μg/ml, 10 min) **(C)**, or left untreated **(B)**. The free dye was washed off and images were captured. Formaldehyde-fixed and permeabilized cells were stained with anti-Golgin-97 (1 μg/ml) / anti-mouse-IgG-Cy3 **(B)** to stain the Golgi compartment **(B)**. ACAT vesicles are shown by their green GFP fluorescence **(A–C)**. Similar staining patterns were observed in >100 cells (n = 2). (Bars, 10 μm).

SUPPLEMENTARY FIGURE S4
Colocalization of ACAT vesicles with organelle-specific markers. HEK-ACAT cells **(A,C)** or HEK cells stably co-expressing encoding ACAT-GFP and DsRed-Peroxi (with "SKL" targeting signal) **(B)** were treated with eflucimibe for 1 h. To visualize mitochondria, living cells were incubated with Mitotracker CMTMROs (200 nM, 10 min, 30°C) **(A)**. The free dye was washed off and images were captured after fixation with formaldehyde. Peroxisomes were detected in formaldehyde-fixed HEK cells co-expressing ACAT-GFP and DsRed-Peroxi by capturing the fluorescence of DsRed **(B)**. Formaldehyde-fixed and permeabilized HeLa-ACAT cells were incubated with anti-sec31 / anti-mouse-IgG-Cy3 to stain ER exit sites **(C)**. ACAT vesicles are shown by their green GFP fluorescence **(A–C)**. Similar staining patterns were observed in >100 cells (n = 2) (Bars, 10 μm) in **(A,B)**, 5 μm in **(C)**.

References

Area-Gomez, E., Del Carmen Lara, C. M., Tambini, M. D., Guardia-Laguarta, C., de Groof, A. J., Madra, M., et al. (2012). Upregulated function of mitochondria-associated ER membranes in Alzheimer disease. *EMBO J.* 31, 4106–4123. doi:10.1038/emboj.2012.202

Bandyopadhyay, S., Li, J., Traer, E., Tyner, J. W., Zhou, A., Oh, S. T., et al. (2017). Cholesterol esterification inhibition and imatinib treatment synergistically inhibit growth of BCR-ABL mutation-independent resistant chronic myelogenous leukemia. *PLoS.One.* 12, e0179558. doi:10.1371/journal.pone.0179558

Batetta, B., Mulas, M. F., Sanna, F., Putzolu, M., Bonatesta, R. R., Gasperi-Campani, A., et al. (2003). Role of cholesterol ester pathway in the control of cell cycle in human aortic smooth muscle cells. *FASEB J.* 17, 746–748. doi:10.1096/fj.02-0396fje

Bligh, E. D., and Dyer, W. J. (1959). A rapid method of total lipid extraction and purification. *Canad. J. Biochem. Physiol.* 37, 911–917. doi:10.1139/o59-099

Brown, D. A. (2001). Lipid droplets: proteins floating on a pool of fat. *Curr. Biol.* 11, R446–R449. doi:10.1016/s0960-9822(01)00257-3

Brown, M. S., Radhakrishnan, A., and Goldstein, J. L. (2018). Retrospective on cholesterol homeostasis: the central role of scap. *Annu. Rev. Biochem.* 87, 783–807. doi:10.1146/annurev-biochem-062917-011852

Chang, C. C., Doolittle, G. M., and Chang, T. Y. (1986). Cycloheximide sensitivity in regulation of acyl coenzyme A:cholesterol acyltransferase activity in Chinese hamster ovary cells. 1. Effect of exogenous sterols. *Biochemistry* 25, 1693–1699. doi:10.1021/bi00355a038

Chang, C. C., Lee, C. Y., Chang, E. T., Cruz, J. C., Levesque, M. C., and Chang, T. Y. (1998). Recombinant acyl-CoA:cholesterol acyltransferase-1 (ACAT-1) purified to essential homogeneity utilizes cholesterol in mixed micelles or in vesicles in a highly cooperative manner. *J. Biol. Chem.* 273, 35132–35141. doi:10.1074/jbc.273.52.35132

Chang, C. C., Miyazaki, A., Dong, R., Kheirollah, A., Yu, C., Geng, Y., et al. (2010). Purification of recombinant acyl-coenzyme A:cholesterol acyltransferase 1 (ACAT1) from H293 cells and binding studies between the enzyme and substrates using difference intrinsic fluorescence spectroscopy. *Biochemistry* 49, 9957–9963. doi:10.1021/bi1013936

Chang, T. Y., Chang, C. C., Lin, S., Yu, C., Li, B. L., and Miyazaki, A. (2001a). Roles of acyl-coenzyme A:cholesterol acyltransferase-1 and -2. *Curr. Opin. Lipidol.* 12, 289–296. doi:10.1097/00041433-200106000-00008

Chang, T. Y., Chang, C. C., Lu, X., and Lin, S. (2001b). Catalysis of ACAT may be completed within the plane of the membrane: a working hypothesis. *J.Lipid Res.* 42, 1933–1938. doi:10.1016/s0022-2275(20)31521-2

Chang, T. Y., Chang, C. C. Y., Harned, T. C., De La Torre, A. L., Lee, J., Huynh, T. N., et al. (2021). Blocking cholesterol storage to treat Alzheimer's disease. *Explor. Neuroprotective. Ther.* 1, 173–184. doi:10.37349/ent.2021.00014

Charles, K. N., Shackelford, J. E., Faust, P. L., Fliesler, S. J., Stangl, H., and Kovacs, W. J. (2020). Functional peroxisomes are essential for efficient cholesterol sensing and synthesis. *Front. Cell Dev.Biol.* 8, 560266. doi:10.3389/fcell.2020.560266

Cheng, D., Chang, C. C., Qu, X., and Chang, T. Y. (1995). Activation of acyl-coenzyme A:cholesterol acyltransferase by cholesterol or by oxysterol in a cell-free system. *J. Biol. Chem.* 270, 685–695. doi:10.1074/jbc.270.2.685

Chornyi, S., Ijlst, L., van Roermund, C. W. T., Wanders, R. J. A., and Waterham, H. R. (2020). Peroxisomal metabolite and cofactor transport in humans. *Front. Cell Dev.Biol.* 8, 613892. doi:10.3389/fcell.2020.613892

Chu, B. B., Liao, Y. C., Qi, W., Xie, C., Du, X., Wang, J., et al. (2015). Cholesterol transport through lysosome-peroxisome membrane contacts. *Cell* 161, 291–306. doi:10.1016/j.cell.2015.02.019

Corvera, S., DiBonaventura, C., and Shpetner, H. S. (2000). Cell confluence-dependent remodeling of endothelial membranes mediated by cholesterol. *J. Biol. Chem.* 275, 31414–31421. doi:10.1074/jbc.M001708200

Das, A., Brown, M. S., Anderson, D. D., Goldstein, J. L., and Radhakrishnan, A. (2014). Three pools of plasma membrane cholesterol and their relation to cholesterol homeostasis. *Elife* 3, e02882. doi:10.7554/eLife.02882

de Medina, P., Genovese, S., Paillasse, M. R., Mazaheri, M., Caze-Subra, S., Bystricky, K., et al. (2010). Auraptene is an inhibitor of cholesterol esterification and a modulator of estrogen receptors. *Mol. Pharmacol.* 78, 827–836. doi:10.1124/mol.110.065250

de Medina, P., Payre, B. L., Bernad, J., Bosser, I., Pipy, B., Silvente-Poirot, S., et al. (2004). Tamoxifen is a potent inhibitor of cholesterol esterification and prevents the formation of foam cells. *J. Pharmacol. Exp. Ther.* 308, 1165–1173. doi:10.1124/jpet.103.060426

Dessi, S., Batetta, B., Pani, A., Spano, O., Sanna, F., Putzolu, M., et al. (1997). Role of cholesterol synthesis and esterification in the growth of CEM and MOLT4 lymphoblastic cells. *Biochem. J.* 321 (3), 603–608. doi:10.1042/bj3210603

Du, X., Pham, Y. H., and Brown, A. J. (2004). Effects of 25-hydroxycholesterol on cholesterol esterification and sterol regulatory element-binding protein processing are dissociable: implications for cholesterol movement to the regulatory pool in the endoplasmic reticulum. *J. Biol. Chem.* 279, 47010–47016. doi:10.1074/jbc.M408690200

Ercan, B., Naito, T., Koh, D. H. Z., Dharmawan, D., and Saheki, Y. (2021). Molecular basis of accessible plasma membrane cholesterol recognition by the GRAM domain of GRAMD1b. *EMBO J.* 40, e106524. doi:10.15252/embj.2020106524

Fuellekrug, J., Ehehalt, R., and Poppelreuther, M. (2012). Outlook: membrane junctions enable the metabolic trapping of fatty acids by intracellular acyl-CoA synthetases. *Front. Physiol.* 3, 401. doi:10.3389/fphys.2012.00401

Gimpl, G., Burger, K., and Fahrenholz, F. (1997). Cholesterol as modulator of receptor function. *Biochemistry* 36, 10959–10974. doi:10.1021/bi963138w

Giovannoni, M. P., Piaz, V. D., Vergelli, C., and Barlocco, D. (2003). Selective ACAT inhibitors as promising antihyperlipidemic, antiathero-sclerotic and anti-Alzheimer drugs. *Mini. Rev. Med. Chem.* 3, 576–584. doi:10.2174/1389557033487890

Guan, C., Niu, Y., Chen, S. C., Kang, Y., Wu, J. X., Nishi, K., et al. (2020). Structural insights into the inhibition mechanism of human sterol O-acyltransferase 1 by a competitive inhibitor. *Nat. Commun.* 11, 2478. doi:10.1038/s41467-020-16288-4

Harned, T. C., Stan, R. V., Cao, Z., Chakrabarti, R., Higgs, H. N., Chang, C. C. Y., et al. (2023). Acute ACAT1/SOAT1 blockade increases MAM cholesterol and strengthens ER-mitochondria connectivity. *Int. J. Mol. Sci.* 24, 5525. doi:10.3390/ijms24065525

Hutter-Paier, B., Huttunen, H. J., Puglielli, L., Eckman, C. B., Kim, D. Y., Hofmeister, A., et al. (2004). The ACAT inhibitor CP-113,818 markedly reduces amyloid pathology in a mouse model of Alzheimer's disease. *Neuron* 44, 227–238. doi:10.1016/j.neuron.2004.08.043

Huttunen, H. J., Greco, C., and Kovacs, D. M. (2007). Knockdown of ACAT-1 reduces amyloidogenic processing of APP. *FEBS Lett.* 581, 1688–1692. doi:10.1016/j.febslet.2007.03.056

Ikonen, E. (2008). Cellular cholesterol trafficking and compartmentalization. *Nat.Rev.Mol.Cell Biol.* 9, 125–138. doi:10.1038/nrm2336

Junquero, D., Bruniquel, F., N'Guyen, X., Autin, J. M., Patoiseau, J. F., Degryse, A. D., et al. (2001a). F 12511, a novel ACAT inhibitor, and atorvastatin regulate endogenous hypercholesterolemia in a synergistic manner in New Zealand rabbits fed a casein-enriched diet. *Atherosclerosis* 155, 131–142. doi:10.1016/s0021-9150(00)00559-1

Junquero, D., Pilon, A., Carilla-Durand, E., Patoiseau, J. F., Tarayre, J. P., Torpier, G., et al. (2001b). Lack of toxic effects of F 12511, a novel potent inhibitor of acyl-coenzyme A: cholesterol O-acyltransferase, on human adrenocortical cells in culture. *Biochem. Pharmacol.* 61, 387–398. doi:10.1016/s0006-2952(00)00555-4

Kamikawa, M., Lei, X., Fujiwara, Y., Nishitsuji, K., Mizuta, H., Takeya, M., et al. (2014). ACAT1-associated late endosomes/lysosomes significantly improve impaired intracellular cholesterol metabolism and the survival of niemann-pick type C mice. *Acta histochem. Cytochem.* 47, 35–43. doi:10.1267/ahc.13033

Kawasaki, T., Maeda, M., and Tsuji, A. (1982). Determination of 17-hydroxycorticosteroids in urine by fluorescence high-performance liquid chromatography using Dns-hydrazine as a pre-column labeling reagent. *J. Chromatogr.* 232, 1–11. doi:10.1016/s0378-4347(00)86001-6

Ke, H., Luan, Y., Wu, S., Zhu, Y., and Tong, X. (2021). The role of mondo family transcription factors in nutrient-sensing and obesity. *Front. Endocrinol.(Lausanne)* 12, 653972. doi:10.3389/fendo.2021.653972

Khelef, N., Soe, T. T., Quehenberger, O., Beatini, N., Tabas, I., and Maxfield, F. R. (2000). Enrichment of acyl coenzyme A:cholesterol O-acyltransferase near trans-golgi network and endocytic recycling compartment. *Arterioscler. Thromb. Vasc. Biol.* 20, 1769–1776. doi:10.1161/01.atv.20.7.1769

Lange, Y., Swaisgood, M. H., Ramos, B. V., and Steck, T. L. (1989). Plasma membranes contain half the phospholipid and 90% of the cholesterol and sphingomyelin in cultured human fibroblasts. *J. Biol. Chem.* 264, 3786–3793. doi:10.1016/s0021-9258(19)84918-9

Lange, Y., Tabei, S. M., Ye, J., and Steck, T. L. (2013). Stability and stoichiometry of bilayer phospholipid-cholesterol complexes: relationship to cellular sterol distribution and homeostasis. *Biochemistry* 52, 6950–6959. doi:10.1021/bi400862q

Lange, Y., Ye, J., and Steck, T. L. (2004). How cholesterol homeostasis is regulated by plasma membrane cholesterol in excess of phospholipids. *Proc. Natl. Acad. Sci. U.S.A* 101, 11664–11667. doi:10.1073/pnas.0404766101

Lee, H. T., Sliskovic, D. R., Picard, J. A., Roth, B. D., Wierenga, W., Hicks, J. L., et al. (1996). Inhibitors of acyl-CoA: cholesterol O-acyl transferase (ACAT) as hypocholesterolemic agents. CI-1011: an acyl sulfamate with unique cholesterol-lowering activity in animals fed noncholesterol-supplemented diets. *J. Med. Chem.* 39, 5031–5034. doi:10.1021/jm960674d

Lei, X., Fujiwara, Y., Chang, C. C., Chang, T. Y., Takeya, M., and Sakashita, N. (2010). Association of ACAT1-positive vesicles with late endosomes/lysosomes in cholesterol-rich human macrophages. *J. Atheroscler. Thromb.* 17, 740–750. doi:10.5551/jat.4416

Li, J., Qu, X., Tian, J., Zhang, J. T., and Cheng, J. X. (2018). Cholesterol esterification inhibition and gemcitabine synergistically suppress pancreatic ductal adenocarcinoma proliferation. *PLoS.One.* 13, e0193318. doi:10.1371/journal.pone.0193318

Li, L., and Pownall, H. J. (2000). Regulation of acyl-coenzyme A:cholesterol acyltransferase (ACAT) synthesis, degradation, and translocation by high-density lipoprotein(2) at a low concentration. *Arterioscler. Thromb. Vasc. Biol.* 20, 2636–2642. doi:10.1161/01.atv.20.12.2636

Lin, S., Lu, X., Chang, C. C., and Chang, T. Y. (2003). Human acyl-coenzyme A: cholesterol acyltransferase expressed in Chinese hamster ovary cells: membrane topology and active site location. *Mol. Biol. Cell.* 14, 2447–2460. doi:10.1091/mbc.e02-11-0725

Liu, P., Ying, Y., Zhao, Y., Mundy, D. I., Zhu, M., and Anderson, R. G. (2004). Chinese hamster ovary K2 cell lipid droplets appear to be metabolic organelles involved in membrane traffic. *J. Biol. Chem.* 279, 3787–3792. doi:10.1074/jbc.M311945200

Llaverias, G., Laguna, J. C., and Alegret, M. (2003). Pharmacology of the ACAT inhibitor avasimibe (CI-1011). *Cardiovasc.Drug Rev.* 21, 33–50. doi:10.1111/j.1527-3466.2003.tb00104.x

Maiwald, A., Bauer, O., and Gimpl, G. (2017). Synthesis and characterization of a novel rhodamine labeled cholesterol reporter. *Biochim.Biophys.Acta Biomembr.* 1859, 1099–1113. doi:10.1016/j.bbamem.2017.02.018

Matsuda, D., Ohte, S., Ohshiro, T., Jiang, W., Rudel, L., Hong, B., et al. (2008). Molecular target of piperine in the inhibition of lipid droplet accumulation in macrophages. *Biol. Pharm. Bull.* 31, 1063–1066. doi:10.1248/bpb.31.1063

Maxfield, F. R., and Tabas, I. (2005). Role of cholesterol and lipid organization in disease. *Nature* 438, 612–621. doi:10.1038/nature04399

Mejhert, N., Kuruvilla, L., Gabriel, K. R., Elliott, S. D., Guie, M. A., Wang, H., et al. (2020). Partitioning of MLX-family transcription factors to lipid droplets regulates metabolic gene expression. *Mol. Cell.* 77, 1251–1264. doi:10.1016/j.molcel.2020.01.014

Murphy, D. J., and Vance, J. (1999). Mechanisms of lipid-body formation. *Trends biochem. Sci.* 24, 109–115. doi:10.1016/s0968-0004(98)01349-8

Naito, T., Ercan, B., Krshnan, L., Triebl, A., Koh, D. H. Z., Wei, F. Y., et al. (2019). Movement of accessible plasma membrane cholesterol by the GRAMD1 lipid transfer protein complex. *Elife* 8, e51401. doi:10.7554/eLife.51401

Ohvo-Rekila, H., Ramstedt, B., Leppimaki, P., and Slotte, J. P. (2002). Cholesterol interactions with phospholipids in membranes. *Prog.Lipid Res.* 41, 66–97. doi:10.1016/s0163-7827(01)00020-0

Olzmann, J. A., and Carvalho, P. (2019). Dynamics and functions of lipid droplets. *Nat.Rev.Mol.Cell Biol.* 20, 137–155. doi:10.1038/s41580-018-0085-z

Qian, H., Zhao, X., Yan, R., Yao, X., Gao, S., Sun, X., et al. (2020). Structural basis for catalysis and substrate specificity of human ACAT1. *Nature* 581, 333–338. doi:10.1038/s41586-020-2290-0

Radhakrishnan, A., and McConnell, H. M. (2000). Chemical activity of cholesterol in membranes. *Biochemistry* 39, 8119–8124. doi:10.1021/bi0005097

Ren, M., Xu, H., Xia, H., Tang, Q., and Bi, F. (2021). Simultaneously targeting SOAT1 and CPT1A ameliorates hepatocellular carcinoma by disrupting lipid homeostasis. *Cell death. Discov.* 7, 125. doi:10.1038/s41420-021-00504-1

Rogers, M. A., Chang, C. C. Y., Maue, R. A., Melton, E. M., Peden, A. A., Garver, W. S., et al. (2022). Acat1/Soat1 knockout extends the mutant Npc1 mouse lifespan and ameliorates functional deficiencies in multiple organelles of mutant cells. *Proc. Natl. Acad. Sci. U.S.A* 119, e2201646119. doi:10.1073/pnas.2201646119

Rogers, M. A., Liu, J., Kushnir, M. M., Bryleva, E., Rockwood, A. L., Meikle, A. W., et al. (2012). Cellular pregnenolone esterification by acyl-CoA:cholesterol acyltransferase. *J. Biol. Chem.* 287, 17483–17492. doi:10.1074/jbc.M111.331306

Rogers, M. A., Liu, J., Song, B. L., Li, B. L., Chang, C. C., and Chang, T. Y. (2015). Acyl-CoA:cholesterol acyltransferases (ACATs/SOATs): enzymes with multiple sterols as substrates and as activators. *J.Steroid Biochem.Mol.Biol.* 151, 102–107. doi:10.1016/j.jsbmb.2014.09.008

Sakashita, N., Chang, C. C., Lei, X., Fujiwara, Y., Takeya, M., and Chang, T. Y. (2010). Cholesterol loading in macrophages stimulates formation of ER-derived vesicles with elevated ACAT1 activity. *J.Lipid Res.* 51, 1263–1272. doi:10.1194/jlr.M900288

Sandhu, J., Li, S., Fairall, L., Pfisterer, S. G., Gurnett, J. E., Xiao, X., et al. (2018). Aster proteins facilitate nonvesicular plasma membrane to ER cholesterol transport in mammalian cells. *Cell* 175, 514–529. doi:10.1016/j.cell.2018.08.033

Schaegger, H., and von Jagow, G. (1991). Blue native electrophoresis for isolation of membrane protein complexes in enzymatically active form. *Anal. Biochem.* 199, 223–231. doi:10.1016/0003-2697(91)90094-a

Suzuki, M., Ohsaki, Y., Tatematsu, T., Shinohara, Y., Maeda, T., Cheng, J., et al. (2012). Translation inhibitors induce formation of cholesterol ester-rich lipid droplets. *PLoS.One.* 7, e42379. doi:10.1371/journal.pone.0042379

Tabas, I., and Boykow, G. C. (1987). Protein synthesis inhibition in mouse peritoneal macrophages results in increased acyl coenzyme A:cholesterol acyl transferase activity and cholesteryl ester accumulation in the presence of native low density lipoprotein. *J. Biol. Chem.* 262, 12175–12181. doi:10.1016/s0021-9258(18)45333-1

Takahashi, M., Murate, M., Fukuda, M., Sato, S. B., Ohta, A., and Kobayashi, T. (2007). Cholesterol controls lipid endocytosis through Rab11. *Mol. Biol. Cell.* 18, 2667–2677. doi:10.1091/mbc.e06-10-0924

Targett-Adams, P., Chambers, D., Gledhill, S., Hope, G., Coy, J. F., Girod, A., et al. (2003). Live cell analysis and targeting of the lipid droplet-binding adipocyte differentiation-related protein. *J. Biol. Chem.* 278, 15998–16007. doi:10.1074/jbc.M211289200

Trinh, M. N., Brown, M. S., Goldstein, J. L., Han, J., Vale, G., McDonald, J. G., et al. (2020). Last step in the path of LDL cholesterol from lysosome to plasma membrane to ER is governed by phosphatidylserine. *Proc. Natl. Acad. Sci. U.S.A* 117, 18521–18529. doi:10.1073/pnas.2010682117

Trinh, M. N., Brown, M. S., Seemann, J., Vale, G., McDonald, J. G., Goldstein, J. L., et al. (2022). Interplay between Asters/GRAMD1s and phosphatidylserine in intermembrane transport of LDL cholesterol. *Proc. Natl. Acad. Sci. U.S.A* 119, e2120411119. doi:10.1073/pnas.2120411119

Underwood, K. W., Jacobs, N. L., Howley, A., and Liscum, L. (1998). Evidence for a cholesterol transport pathway from lysosomes to endoplasmic reticulum that is independent of the plasma membrane. *J. Biol. Chem.* 273, 4266–4274. doi:10.1074/jbc.273.7.4266

van Meer, G., Voelker, D. R., and Feigenson, G. W. (2008). Membrane lipids: where they are and how they behave. *Nat.Rev.Mol.Cell Biol.* 9, 112–124. doi:10.1038/nrm2330

Veldhuis, J. D., Strauss, J. F., III, Silavin, S. L., and Kolp, L. A. (1985). The role of cholesterol esterification in ovarian steroidogenesis: studies in cultured swine granulosa cells using a novel inhibitor of acyl coenzyme A: cholesterol acyltransferase. *Endocrinology* 116, 25–30. doi:10.1210/endo-116-1-25

Walther, T. C., Chung, J., and Farese, R. V., Jr. (2017). Lipid droplet biogenesis. *Annu.Rev.Cell Dev.Biol.* 33, 491–510. doi:10.1146/annurev-cellbio-100616-060608

Websdale, A., Kiew, Y., Chalmers, P., Chen, X., Cioccoloni, G., Hughes, T. A., et al. (2022). Pharmacologic and genetic inhibition of cholesterol esterification enzymes reduces tumour burden: a systematic review and meta-analysis of preclinical models. *Biochem. Pharmacol.* 196, 114731. doi:10.1016/j.bcp.2021.114731

Weger, M., Weger, B. D., Schink, A., Takamiya, M., Stegmaier, J., Gobet, C., et al. (2020). MondoA regulates gene expression in cholesterol biosynthesis-associated pathways required for zebrafish epiboly. *Elife* 9, e57068. doi:10.7554/eLife.57068

Wiegand, V., Chang, T. Y., Strauss, J. F., III, Fahrenholz, F., and Gimpl, G. (2003). Transport of plasma membrane-derived cholesterol and the function of Niemann-Pick C1 Protein. *FASEB J.* 17, 782–784. doi:10.1096/fj.02-0818fje

Wilde, B. R., Kaadige, M. R., Guillen, K. P., Butterfield, A., Welm, B. E., and Ayer, D. E. (2020). Protein synthesis inhibitors stimulate MondoA transcriptional activity by driving an accumulation of glucose 6-phosphate. *Cancer Metab.* 8, 27. doi:10.1186/s40170-020-00233-6

Wing, P. A., Schmidt, N. M., Peters, R., Erdmann, M., Brown, R., Wang, H., et al. (2023). An ACAT inhibitor suppresses SARS-CoV-2 replication and boosts antiviral T cell activity. *PLoS.Pathog.* 19, e1011323. doi:10.1371/journal.ppat.1011323

Xiong, K., Wang, G., Peng, T., Zhou, F., Chen, S., Liu, W., et al. (2021). The cholesterol esterification inhibitor avasimibe suppresses tumour proliferation and metastasis via the E2F-1 signalling pathway in prostate cancer. *Cancer Cell Int.* 21, 461. doi:10.1186/s12935-021-02175-5

Yang, W., Bai, Y., Xiong, Y., Zhang, J., Chen, S., Zheng, X., et al. (2016). Potentiating the antitumour response of CD8(+) T cells by modulating cholesterol metabolism. *Nature* 531, 651–655. doi:10.1038/nature17412

Yue, S., Li, J., Lee, S. Y., Lee, H. J., Shao, T., Song, B., et al. (2014). Cholesteryl ester accumulation induced by PTEN loss and PI3K/AKT activation underlies human prostate cancer aggressiveness. *Cell Metab.* 19, 393–406. doi:10.1016/j.cmet.2014.01.019

Zhu, Y., Gu, L., Lin, X., Zhang, J., Tang, Y., Zhou, X., et al. (2022). Ceramide-mediated gut dysbiosis enhances cholesterol esterification and promotes colorectal tumorigenesis in mice. *JCI.Insight.* 7, e150607. doi:10.1172/jci.insight.150607